Journal of Archaeological Science 36 (2009) 637–652

Contents lists available at ScienceDirect

Journal of Archaeological Science

journal homepage: http://www.elsevier.com/locate/jas

Building a tephrostratigraphic framework for the Paleolithic of Central Anatolia, Turkey

Christian A. Tryon [a,b,*], M. Amelia V. Logan [c], Damase Mouralis [d,e], Steve Kuhn [f], Ludovic Slimak [g], Nur Balkan-Atlı [h]

[a] Department of Anthropology, New York University, 25 Waverly Place, New York, NY 10003, USA
[b] Human Origins Program, Department of Anthropology, National Museum of Natural History, Smithsonian Institution, 10th and Constitution Ave. NW, MRC-112, Washington, DC 20560, USA
[c] Department of Mineral Sciences, National Museum of Natural History, Smithsonian Institution, 10th and Constitution Ave. NW, MRC-119, Washington, DC 20560, USA
[d] Département de Géographie, Université de Rouen, Cedex, France
[e] CNRS (UMR 6266), 76821 Mont St. Aignan, Cedex, France
[f] Department of Anthropology, University of Arizona, Tucson, AZ 85721-0030, USA
[g] CNRS (UMR 5608), TRACES, Université de Toulouse le Mirail, France
[h] Istanbul University, Faculty of Letters, Prehistory Section, Beyazit, 34134, İstanbul, Turkey

ARTICLE INFO

Article history:
Received 18 June 2008
Received in revised form 6 October 2008
Accepted 7 October 2008

Keywords:
Tephra correlation
Middle Paleolithic
Lower Paleolithic
Kaletepe Deresi 3

ABSTRACT

The Central Anatolian Volcanic Province (CAVP) in Turkey preserves widespread deposits of Quaternary tephra, presently associated with a small but growing number of Paleolithic archaeological sites. We use multivariate analyses of the abundances of a suite of nine major and minor element oxides determined by electron probe microanalysis. From these data, we construct a classificatory model for correlating distal tephra to one of five volcanic edifices or eruptive phases within the CAVP. Application of this model to distal deposits of primary tephra-fall and reworked tuffaceous sediments from the archaeological sites of Körkuyu and Kaletepe Deresi 3 indicates Late to possibly Early Pleistocene ages for the artifact assemblages there, and provides a fundamental tephrostratigraphic framework to examine spatial and temporal variation in hominin behavior comparable to that of other regions, such as eastern Africa.

1. Introduction

In regions characterized by active volcanism, pyroclastic deposits from explosive eruptions, or tephra, serve as critical chronological markers because of their wide dispersal, rapid sedimentation, distinct chemical signatures, and amenability to precise radiometric age estimates by a variety of methods (Alloway et al., 2007; Feibel, 1999; Sarna-Wojcicki, 2000). Tephra play a major role in linking paleoenvironmental data from deep sea cores to terrestrial deposits (e.g., deMenocal and Brown, 1999) and provide age constraints for Paleolithic sites and hominin fossil localities in Europe (Anikovich et al., 2007), southern Asia (Petraglia et al., 2007), and particularly in eastern Africa (e.g., Brown et al., 2006; Campisano and Feibel, in press; McHenry et al., 2008; Tryon et al., 2008). We develop here an initial tephrostratigraphic framework for Paleolithic sites in the Central Anatolian Volcanic Province (CAVP) of Turkey (Fig. 1). Multivariate statistical methods are used to distinguish the geochemical signature of eruptives from each of the major Quaternary CAVP volcanoes and to develop a probabilistic classificatory model to assign primary fallout and reworked distal tephra from archaeological sites to these volcanic sources. Central Anatolia is important for testing models of geographic variation in hominin behavior and biology (including dispersals from Africa), but has a relatively short history of investigations of Pleistocene sediments and archaeological sites (Kappelman et al., 2007; Kuhn, 2002; Kuzucuoglu et al., 1998; Mouralis et al., 2002; Otte et al., 1998; Taşkıran, 2008). Because of the dynamic Quaternary geological and tectonic history of Anatolia (Notsu et al., 1995; Taymaz et al., 2007), tephrostratigraphy potentially provides the degree of temporal and spatial resolution required to understand the antiquity and diversity of recently discovered and excavated Paleolithic sites in the region (Slimak et al., 2008).

2. Geological and archaeological context

The Central Anatolian Volcanic Province (CAVP) is part of a still active, rapidly forming collisional orogen that first developed in the

* Corresponding author. Department of Anthropology, New York University, 25 Waverly Place, New York, NY 10003, USA. Tel.: +1 212 992 7475; fax: +1 212 995 4014.
E-mail addresses: christian.tryon@nyu.edu (C.A. Tryon), logana@si.edu (M.A.V. Logan), damase.mouralis@univ-rouen.fr (D. Mouralis), skuhn@email.arizona.edu (S. Kuhn), slimakl@yahoo.fr (L. Slimak), nbalkan@istanbul.edu.tr (N. Balkan-Atlı).

0305-4403/$ – see front matter © 2008 Elsevier Ltd. All rights reserved.
doi:10.1016/j.jas.2008.10.006

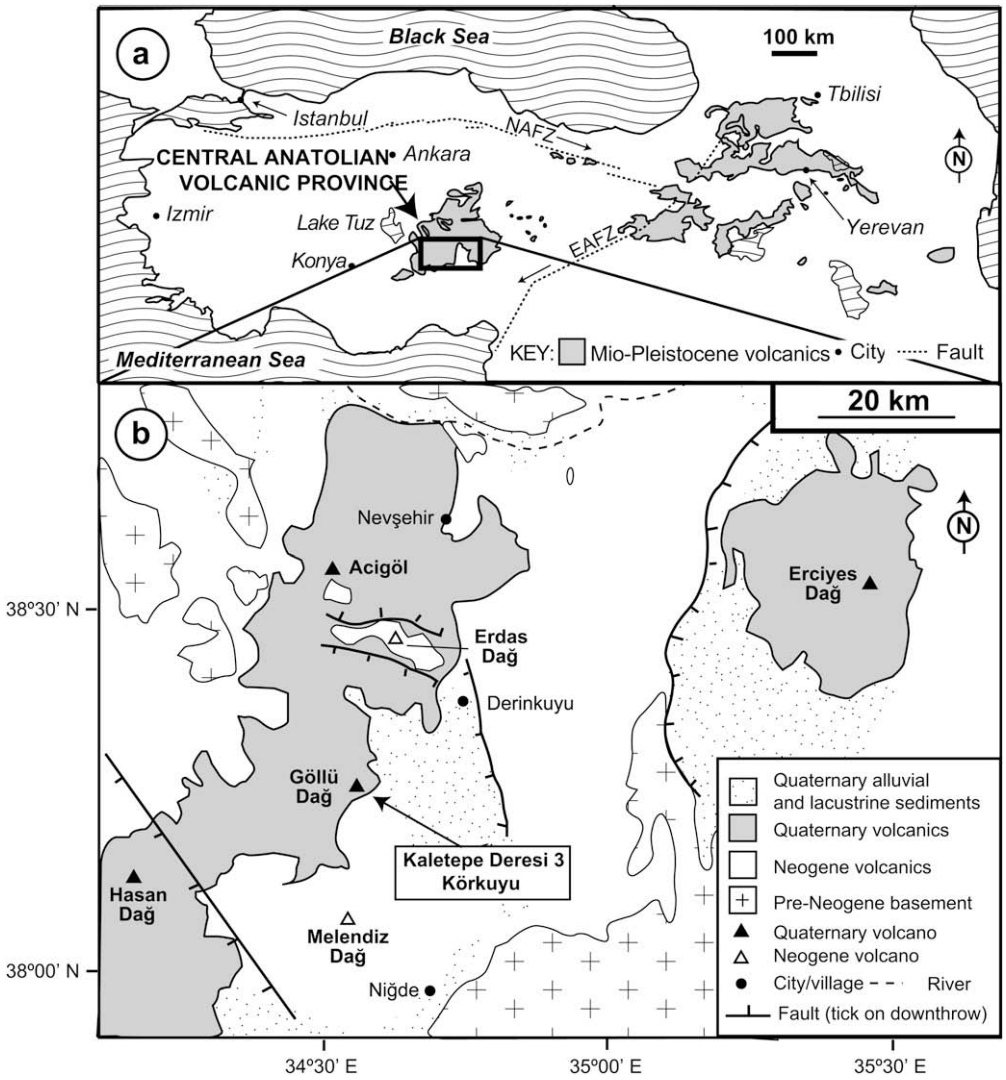

Fig. 1. (a) Schematic map showing the distribution of Quaternary volcanic rocks in Anatolia and adjacent regions and the location of the Central Anatolian Volcanic Province (CAVP), modified from Innocenti et al. (1982) and Deniel et al. (1998). (b) Main geologic features of the CAVP, including all Quaternary volcanic edifices mentioned in the text and relative positions of the archaeological sites Kaletepe Deresi 3 and Körkuyu, after Druitt et al. (1995).

late Oligocene (Pasquarè et al., 1988). The geological and tectonic complexity of the region results from the subduction of the African Plate beneath western Turkey and the Aegean region and the northward motion of the Arabian plate relative to Eurasia (Taymaz et al., 2007). The combination of tectonic forces is causing the Turkish plate to move southward bounded by strike-slip fault zones: The North Anatolian Fault Zone (NAFZ) to the north and the East Anatolian Fault Zone (EAFZ) to the south (Fig. 1a). Associated volcanism in Anatolia is a rare example of arc volcanism related to continental collision, the development of a shortened and thickened continental crust, and resulting alkaline and calc-alkaline magmatism. There are four major Quaternary sources of explosive volcanism in the CAVP that serve as the primary sources of dispersed tephra in the region (Fig. 1b), each with a modest number of fission track and K–Ar dates providing limited chronological control. These include the monogenetic rhyolitic complexes of Göllü Dağ (~1.5–0.4 Ma) and Acigöl (~0.2–0.02 Ma) (Druitt et al., 1995; Mouralis et al., 2002; Slimak et al., 2008) and two basalt–andesite–rhyolite stratovolcanoes, Erciyes Dağ (2.8–0.08 Ma), and Hasan Dağ, the latter particularly poorly dated with explosive activity from ~6.3 Ma to within the last few thousand years, with most present exposures likely dating to the Pleistocene (Aydar and Gourgaud, 1998; Kürkçüoglu et al., 1998). In addition, there are more than 800 smaller predominantly andesitic and basaltic cones, vents, and maars in the area active from ~1.1–0.06 Ma (Notsu et al., 1995; Toprak, 1998).

The archaeological site of Kaletepe Deresi 3 (KD3) occurs within the Gollü Dağ volcanic complex (Fig. 1b). It contains at least five Lower and Middle Paleolithic artifact-bearing strata within reworked tuffaceous sands deposited by fluvial, colluvial, and aeolian processes, exposed in two 4–5 m deep trenches (the *Aval* and *Amont* excavations shown in Figs. 2 and 3). The artifacts overlie rhyolite bedrock K–Ar-dated to 1.1 ± 0.02 Ma (Mouralis, 2003). All archaeological strata except the uppermost (archaeological level I of the *Aval* section in Fig. 3) underlie reworked volcaniclastic sediments that are exposed as minimally reworked tephra-fall deposits ~5 m upstream from the *Amont* excavation (Fig. 2). As detailed elsewhere (Mouralis et al., 2002; Slimak et al., 2004, 2008), these upstream tephra deposits are numbered from bottom to top, with R1–R5 comprising a ~150-cm-thick sequence of closely superimposed 3–25-cm-thick, well-sorted, white-to-light-grey rhyolitic lapilli-fall deposits with minimal post-depositional disturbance. Tephra R1–R5 have been correlated with syn-caldera deposits from Acigöl dating to ~0.16 Ma (Mouralis et al., 2002; Slimak et al., 2004, 2008). An additional bioturbated ~15-cm-thick black-colored trachytic ash-fall deposit (R6) caps the sequence

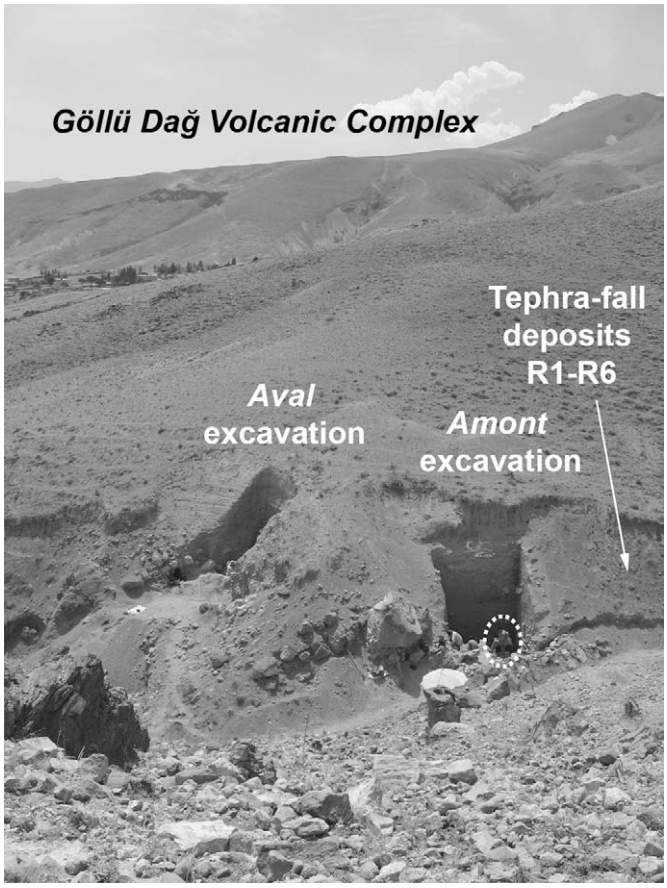

Fig. 2. Photograph of Kaletepe Deresi 3 (KD3), showing the location of the site within the Göllü Dağ volcanic complex. Also shown are the relative positions of the *Aval* and *Amont* excavations in 2006, and the location of exposures of tephra-fall deposits R1–R6. Excavator circled for scale.

exposed adjacent to the *Amont* excavation. It is attributed to the undated monogenetic cone Kurugölkabak Tepe, 15 km north of the site (Mouralis et al., 2002; Slimak et al., 2004, 2008).

KD3 is presently the only excavated Paleolithic site in the CAVP and preserves the only *in situ* Acheulian bifaces in Turkey (within archaeological levels IV–X of Fig. 3). However, recent field surveys have demonstrated the presence of a number of additional Middle Paleolithic sites in the CAVP (e.g., Balkan-Atlı et al., 2008), including Körkuyu, where basalt and obsidian Levallois cores and bifaces are eroding from a paleosol that overlies a well-sorted light-grey lapilli-fall deposit. As described below, samples from both archaeological sites were drawn from tephra-fall deposits and reworked tuffaceous sands, the latter extensively sampled at KD3 by 'geochemical reconnaissance' to isolate tephra that may help narrow the present ~1 million-year age range of the Acheulian strata there (~1.10–0.16 Ma).

3. Tephrostratigraphic methods

We use electron probe microanalysis (EPMA) to determine the major and minor element oxide abundance in volcanic glasses (magma quenched at eruption) and cognate phenocrysts to geochemically characterize tephra deposits. Samples obtained from proximal tephra within each of the four CAVP Quaternary volcanoes form a *reference set* for comparison with distal deposits of unknown source from the archaeological sites of KD3 and Körkuyu. Multivariate statistical analyses are used to distinguish among each member of the reference set and to construct a robust classificatory model for attributing distal deposits at KD3 and Körkuyu to volcanic source in the CAVP.

3.1. Sample collection and preparation

Our reference set consists of analyses of 33 samples of *in situ* proximal tephra fallout and surge deposits from each of the four

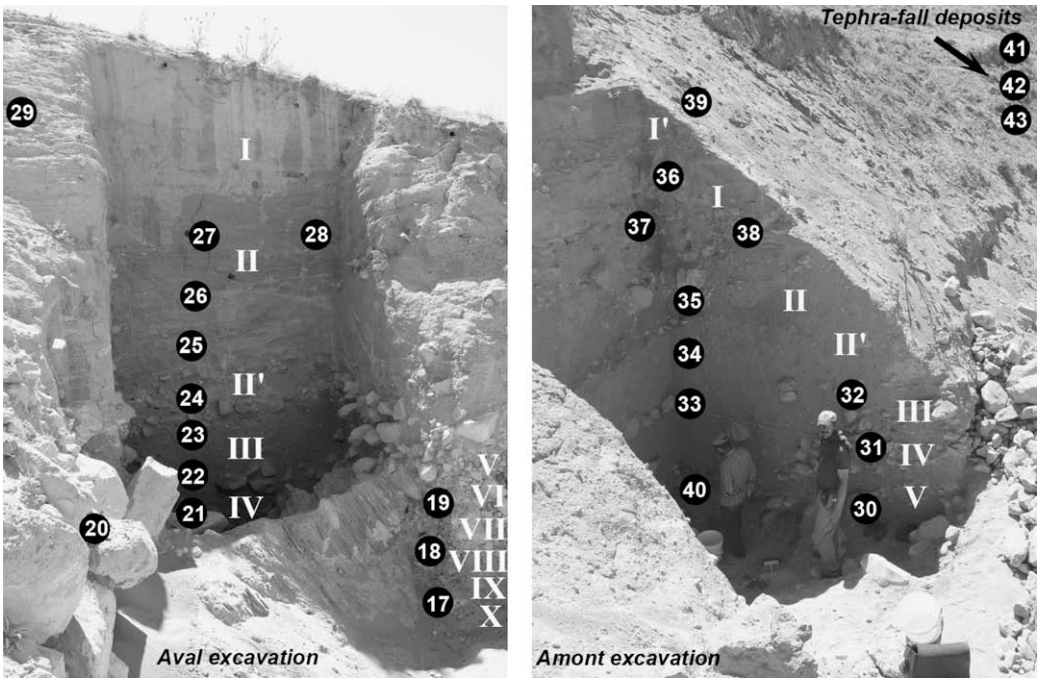

Fig. 3. Photographs of the *Aval* and *Amont* sections of KD3 showing the position of the distal tephra samples collected by Tryon. Arabic numerals in black circles are abbreviated tephra sample numbers (lacking the CAT06- prefix) corresponding to those discussed in text and shown in Tables 5 and 6. Roman numerals show the approximate stratigraphic position of the archaeological levels described by Slimak et al. (2008) for the *Aval* excavation and by Slimak et al. (2004) for the *Amont* excavation. Note that for the *Aval* section, scale is provided by the width of the trench, which is 3 m.

CAVP Quaternary volcanic edifices. It consists of four samples each from Erciyes Dağ and Hasan Dağ, eight from Göllü Dağ, with Acigöl subdivided into 13 samples from syn-caldera deposits and four from post-caldera deposits. Mouralis collected the proximal tephra samples of the reference set for investigating the evolution and eruptive history of each of the CAVP volcanic edifices (for details, see Mouralis, 2003; Mouralis et al., 2002). Our use of these data here are of a different scale and aimed solely at distinguishing among each of the Quaternary CAVP volcanic edifices or major eruptive phases on the basis of major and minor element oxide abundance (Stokes and Lowe, 1988; Stokes et al., 1992).

Tephra-fall deposits R1–R6 were collected by Mouralis from the outcrop adjacent to the KD3 excavations (Fig. 3), with duplicate samples of R4–R6 collected by Tryon. A total of 24 samples were collected by Tryon from both excavated sections at KD3 (Fig. 2). Sampling was from bottom to top at ~50 cm intervals, with additional samples collected as necessary to account for lateral variation within some strata (Fig. 3). One sample was collected by Tryon from Körkuyu. All samples were prepared as grain mounts or where possible due to sediment cohesion, as polished, resin-impregnated, oriented thin sections. For the KD3 sediments, clays were removed from unconsolidated samples by decantation following a 5-min wash in an ultrasonic bath of distilled water. Visual comparison of KD3 sediment thin sections and grain mounts, which consist predominantly of sand-sized glass fragments, showed no obvious difference in grain size, suggesting comparable sampling of the complete size range of clasts for both methods of sample preparation.

3.2. Data acquisition

Wavelength dispersive EPMA of the reference set tephra samples ($n = 347$ analyses) and tephra-fall deposits from KD3 ($n = 66$ analyses) listed in Table 1 was conducted by Mouralis at the Magma and Volcanoes Laboratory in Clermont-Ferrand using a Cameca SX 100 electron microprobe at 15 kV, 6 nA, with a 10 s count time and a 10 μm beam diameter (see Mouralis, 2003; Slimak et al., 2008). Additional samples were collected by Tryon and analyzed by Tryon and Logan, totaling 947 electron probe microanalyses of 481 grains of volcanic glass from a combined set of three of the airfall tephra from KD3 also analyzed by Mouralis, 24 sediment samples from KD3, the airfall tephra from Körkuyu, and one obsidian sample. For these samples, wavelength dispersive quantitative analyses of major and minor element oxide abundance were conducted using a JEOL 8900R electron microprobe, housed in the Mineral Sciences Department of the Smithsonian Institution's National Museum of Natural History, with a 40° takeoff angle. Analytical conditions consisted of an accelerating voltage of 13 kV and a beam current of 10 nA, using a rasterized beam over an area of 25 μm^2. Counting times were 20 s on-peak and 10 s off-peak. Reference materials used for calibration of analyses of the glass and phenocryst phases include anorthite (NMNH 137041), Kakanui hornblende (NMNH 143065), microcline (NMNH 143966), scapolite (NMNH R6600-1), fayalite (NMNH 85276), synthetic wollastonite and enstatite, as well as Yellowstone rhyolitic glass VG-568 (NMNH 7285), characterized by Jarosewich et al. (1980). Raw data were converted to concentrations using standard calculations with a PhiRhoZ matrix correction. Optimal analytical conditions that minimize sample damage and volatile element loss, particularly sodium, were achieved through an extensive testing program of analyzing NMNH 7285 as an unknown (for discussion, see Hunt and Hill, 1996, 2001). A volatile self-correction with a 2 s interval was applied for Na, Si, and K using Probe for Windows software (Donovan, 2006). For the KD3 sediments, selection was non-random, seeking to sample the full spectrum of observed volcanic glass shard morphology, which ranged from highly vesiculated pumiceous fragments to vesicle-poor bubble-wall or bubble-wall-junction shards (Fig. 4). Phenocrysts (including feldspars amenable to age estimation by the $^{40}Ar/^{39}Ar$ or other methods) are rare, with the exception of glasses of basic or intermediate composition (Fig. 4c) and those of the 'KD3 pyroxene tephra' (Fig. 4d) discussed in detail below. In order to obtain representative data for each sample, ~12–20 grains were selected for analysis, with glass from each grain analyzed from 1 to 5 times. Fresh glass shards were selected for analysis using backscattered electron images.

3.3. Data reduction

For the reference set, the volcano (or in the case of Acigöl, the major eruptive phase) is the basic unit of analysis; for tephra-fall deposits R1–R6 from KD3 and that from Körkuyu, the sample

Table 1
Summary data for tephra fallout deposits, listing mean and first standard deviation for each element oxide. The number of electron probe microanalyses is listed for each sample, as is the number of glass shards, each of which was analyzed from 1 to 5 times. Total listed is the sum of the average wt. % of each oxide.

Sample	Shards (n)	Analyses (n)	SiO_2	TiO_2	Al_2O_3	FeO*	MnO	MgO	CaO	Na_2O	K_2O	Total
Reference set: proximal tephra or obsidian												
Acigöl syn-caldera	145	145	72.60 ± 1.76	0.09 ± 0.05	12.96 ± 0.45	1.11 ± 0.14	0.06 ± 0.05	0.09 ± 0.03	0.78 ± 0.07	3.72 ± 0.35	4.37 ± 0.28	95.78
Acigöl post-caldera	43	43	75.11 ± 1.54	0.04 ± 0.04	12.25 ± 0.39	0.70 ± 0.12	0.07 ± 0.05	0.02 ± 0.04	0.39 ± 0.08	4.13 ± 0.21	4.48 ± 0.28	97.19
Göllü Dağ	89	89	73.50 ± 1.19	0.08 ± 0.04	11.94 ± 0.24	0.70 ± 0.11	0.08 ± 0.07	0.03 ± 0.02	0.41 ± 0.06	2.98 ± 0.45	4.65 ± 0.46	94.38
Erciyes Dağ	26	26	73.25 ± 1.04	0.19 ± 0.13	13.37 ± 0.26	1.23 ± 0.11	0.05 ± 0.05	0.24 ± 0.05	1.44 ± 0.12	2.71 ± 0.43	3.36 ± 0.13	95.83
Hasan Dağ	44	44	75.45 ± 1.51	0.19 ± 0.08	12.65 ± 0.66	0.99 ± 0.19	0.04 ± 0.05	0.19 ± 0.06	0.90 ± 0.20	2.41 ± 0.82	3.78 ± 0.50	96.61
Obsidian	4	12	77.83 ± 0.86	0.05 ± 0.01	12.83 ± 0.13	0.74 ± 0.15	0.06 ± 0.03	0.03 ± 0.01	0.45 ± 0.03	4.07 ± 0.18	4.48 ± 0.16	100.55
Distal tephra-fall deposits												
CAT06-41T = R6	15	20	61.05 ± 1.11	1.94 ± 0.16	14.72 ± 0.97	7.40 ± 0.72	0.15 ± 0.04	*2.02 ± 0.28*	*4.36 ± 0.43*	4.32 ± 0.25	*2.79 ± 0.29*	98.75
C2D14 - R6	14	14	62.19 ± 2.44	1.78 ± 0.22	14.04 ± 0.42	6.35 ± 1.09	0.12 ± 0.04	*1.47 ± 0.32*	*3.60 ± 0.51*	4.56 ± 0.59	*3.13 ± 0.41*	97.24
CAT06-42T = R5	13	35	*73.49 ± 0.95*	0.07 ± 0.01	*12.91 ± 0.12*	0.93 ± 0.16	0.05 ± 0.03	0.05 ± 0.01	0.70 ± 0.04	3.77 ± 0.20	4.35 ± 0.25	96.34
C3D8 - R5	6	6	*71.37 ± 0.56*	0.11 ± 0.04	*12.51 ± 0.18*	0.97 ± 0.06	0.05 ± 0.04	0.07 ± 0.02	0.73 ± 0.12	3.78 ± 0.15	4.54 ± 0.29	94.14
CAT06-43T = R4	12	35	*73.44 ± 1.06*	0.08 ± 0.02	12.66 ± 0.24	0.91 ± 0.18	0.05 ± 0.03	0.05 ± 0.01	0.71 ± 0.09	3.76 ± 0.20	4.37 ± 0.22	96.04
C2D12 - R4	10	10	*72.14 ± 0.35*	0.08 ± 0.04	12.45 ± 0.13	0.92 ± 0.09	0.04 ± 0.03	0.08 ± 0.04	0.72 ± 0.06	3.71 ± 0.22	4.49 ± 0.18	94.64
C2D11 - R3	12	12	74.42 ± 2.24	0.07 ± 0.05	12.54 ± 0.31	0.81 ± 0.20	0.03 ± 0.04	0.06 ± 0.03	0.64 ± 0.15	3.87 ± 0.26	4.78 ± 0.49	97.22
C3D4 - R2	7	7	72.75 ± 0.53	0.05 ± 0.03	12.38 ± 0.12	0.92 ± 0.12	0.05 ± 0.06	0.06 ± 0.04	0.72 ± 0.09	3.68 ± 0.15	4.54 ± 0.15	95.15
C2D8 - R1	17	17	72.99 ± 1.83	0.09 ± 0.06	12.60 ± 0.40	0.86 ± 0.18	0.06 ± 0.05	0.05 ± 0.03	0.70 ± 0.08	3.88 ± 0.24	4.50 ± 0.16	95.73
CAT06-46T (Körkuyu)	18	54	74.68 ± 0.93	0.05 ± 0.02	12.39 ± 0.11	0.66 ± 0.15	0.07 ± 0.03	0.02 ± 0.01	0.38 ± 0.05	3.81 ± 0.16	4.44 ± 0.16	96.50
Cryptotephra												
KD3 pyroxene tephra	30	71	73.64 ± 1.30	0.15 ± 0.02	12.11 ± 0.32	0.96 ± 0.16	0.04 ± 0.02	0.15 ± 0.03	0.90 ± 0.09	3.36 ± 0.28	3.79 ± 0.15	95.10

*Total Fe expressed as FeO. Note that the analytical results for samples C2D14, C3D8, C2D12, C2D11, C3D4, and C2D8 were previously published in Slimak et al. (2008) and are reported here for comparison. Italic values represent element oxide abundances with mean values that do not overlap at one standard deviation among the inter-laboratory comparisons.

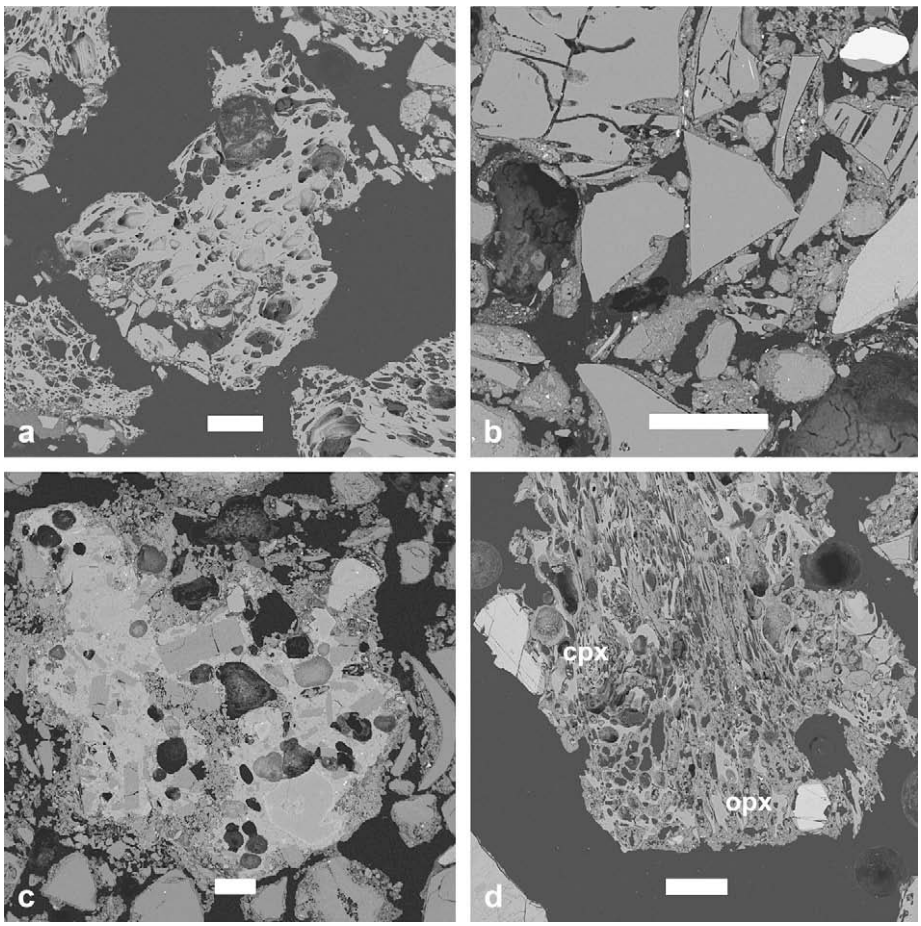

Fig. 4. Backscattered electron images of vitric grains from Kaletepe Deresi 3 sediments showing morphological variation: (a) rhyolitic vesicular pyroclasts from CAT06-38T, (b) rhyolitic vesicle-poor pyroclasts from CAT06-29T, (c) weathered basaltic pyroclast from CAT-35T, and (d) clinopyroxene- (cpx) and orthopyroxene- (opx) bearing rhyolitic vesicular pyroclast of the 'KD3 pyroxene tephra' from CAT06-33T. Note that these phenocrysts are smaller than many assigned to this deposit. All scale bars are 100 μm in length.

(or bed) is used as the basic unit of analysis. In both cases, these aggregate data are characterized by the mean and first standard deviation of each analyzed element oxide, and are reported in Table 1. For the reworked KD3 sediments, the individual grain (or shard) is used as the unit of analysis. Because of minimal intra-grain variation and to facilitate multivariate analyses of the data, each grain is characterized by the average value for each element oxide. The dataset was further culled by removing analyses with analytical totals $< 90\%$, following the range of acceptable values noted by Froggatt (1992; see also Pearce et al., 2008). Data are not normalized except where required for comparison with whole-rock analyses (e.g., when plotted on the total-alkali-silica diagram), in part because of some of the unwarranted assumptions this makes about the parent magma, but more importantly because such treatment of the data has little to no effect on the discriminant analyses used here (see discussions in Brown et al., 1992; Hunt and Hill, 1993; Charman and Grattan, 1999; Pearce et al., 2007).

Sample position on the total-alkali-silica diagram (TAS) of Le Bas et al. (1986) was used to identify major compositional groups. Glasses of basic (basaltic–andesitic) and intermediate (andesitic–trachytic) composition are treated separately because of their rarity within the samples studied here and the paucity of comparative data within the CAVP. The main focus was upon shards of acidic (rhyolitic) composition. The sample means of multiple element oxides overlap at one standard deviation among the eruptive phases and sources that comprise the reference set (Table 1; Fig. 5). Even this degree of overlap has not limited attribution of tephra to the syn-caldera phase of Acigöl (e.g., Slimak et al., 2008), but geochemical compositional separation is insufficient to reliably distinguish among the other volcanic sources or eruptive phases of the reference set. Because traditional approaches using bivariate plots fail to produce consistent source separation, we adopt a multivariate approach that allows for the probabilistic determination of the volcanic source of distal tephra deposits (Stokes and Lowe, 1988; Stokes et al., 1992; Charman and Grattan, 1999; Pollard et al., 2006), appropriate, as discussed below, for combined sets of data generated by multiple laboratories.

3.4. Multivariate statistical methods

Building on initial efforts by Mouralis (2003), canonical variates analysis was employed to reduce and graphically interpret observed variation within the reference set using the pooled-within canonical structure. Using data from the reference set, linear discriminant analysis was used to construct a classificatory model for rhyolitic distal tephra of undetermined source. Models were generated using two software packages, SAS Version 9.1 for Windows (© 2002–2003 SAS Institute, Inc., Cary, NC, USA) and SYSTAT Version 11.0 for Windows (© 2004 SYSTAT Software, Inc., San Jose, CA, USA), using an iterative approach to identify the statistical method with the lowest probabilities of misclassification as estimated by the cross-validation method (Johnson and Wichern, 2002). Data from all analyzed element oxides are used; stepwise approaches are not used because they excluded at most one element oxide (MnO), resulted in higher probabilities of misclassification, and generally require more assumptions and

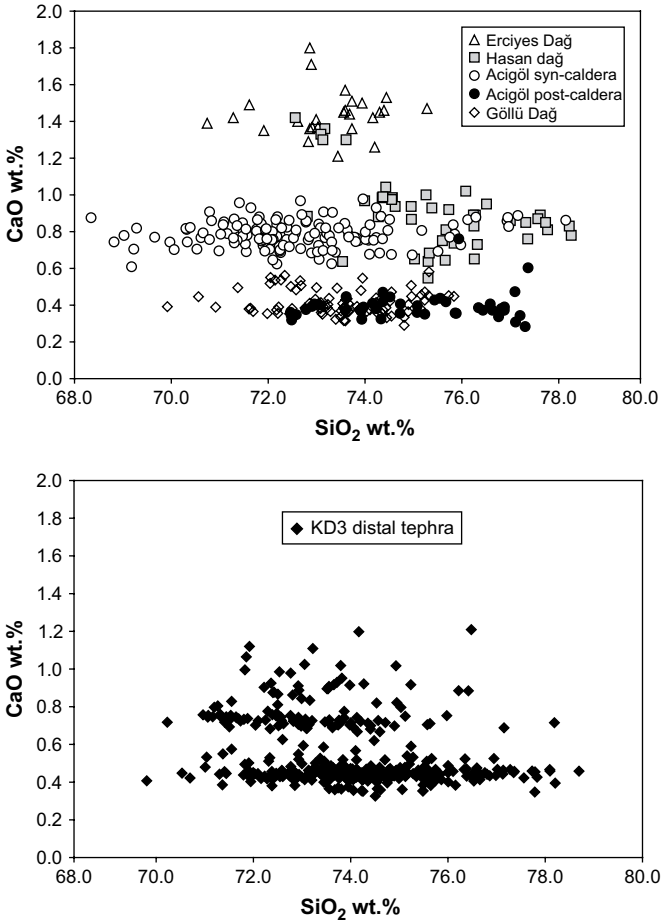

Fig. 5. Bivariate plots of SiO_2 and CaO wt. % of Central Anatolian Volcanic Province tephra using untransformed data, showing generally poor separation among volcanic sources (upper plot) and the range of compositional variation among distal tephra (primary fallout and reworked) at Kaletepe Deresi 3.

result in less robust classification models (Baxter, 1994b). Prior probabilities were weighted proportionately due to group size differences within our sample. Untransformed data are used here due to the higher posterior probabilities of group membership relative to data transformed by normalization or the centered log ratio method of Aitchison (1986), the latter used in some provenance studies based on geochemical data with varying degrees of success (see discussions in Stokes et al., 1992; Baxter et al., 2005; Pearce et al., 2008; Pollard et al., 2006).

This classificatory model was used to assign distal tephra deposits from archaeological sites to one of the volcanic sources or eruptive phases within the reference set: Erciyes Dağ, Hasan Dağ, Göllü Dağ, or the syn-caldera or post-caldera deposits from Acigöl. Within our current reference set, geochemical compositional contrasts among different volcanic sources are substantially greater than variation within each source (see also, Stokes and Lowe, 1988; Stokes et al., 1992), and thus at present we attempt correlations only at the broad scale of attributing distal tephra to source volcano (or major eruptive phase in the case of Acigöl). In our examination of the reworked tuffaceous sediments from KD3, analyses of obsidian grains (sample CAT06-18T) from the *Aval* excavation (Figs. 2 and 3) were also added to the basic classificatory model. This was done to assess the proportion of obsidian fragments within the sediments eroding from outcrops upstream (see Poidevin, 1998 for a summary). Obsidian is (rhyolitic) volcanic glass, and sand-sized fragments may be visually indistinguishable from blocky glass shards (as opposed to pumiceous grains) deposited as tephra.

Inspection of canonical variates plots, Mahalanobis distances, and associated posterior probabilities are used to estimate the likelihood of a classification. We adopt a very conservative approach in our classification of distal tephra in general, and particularly for the reworked sediments from KD3, for two reasons. First, our reference set of rhyolitic glasses is comprehensive but incomplete, given the additional smaller volcanic edifices within the CAVP (Toprak, 1998) that may have contributed to the tuffaceous sediments at KD3. Second, discriminant analysis assigns each sample/grain to one of the five or six potential sources/eruptive phases, with classification determined on the basis of the lowest Mahalanobis distance and highest posterior probability. Importantly, there is no absolute measure of strength, nor is there a guarantee that the attribution is correct, only that the assigned source has the highest probability of being correct *within the current reference set* (e.g., Baxter, 1994a: 202). Additional analyses of samples from any of the major Quaternary CAVP volcanic edifices would expand the reference set and may alter the resolution of our correlations. However, recognizing the limits of our present dataset, we consider the strongest potential correlates those samples or individual grains that are classified to a particular source with ≥95% posterior probability and plot within the multivariate space defined by the canonical variates for that source.

4. Tephrostratigraphic results

4.1. A discriminant model for the major CAVP Quaternary rhyolitic eruptive phases

Table 1 summarizes the EPMA results from proximal tephra from Göllü Dağ, Hasan Dağ, Erciyes Dağ, Acigöl syn-caldera, and post-caldera eruptive phases that form the reference set. Inspection of canonical variates (CV) plots shows good separation among the different sources and eruptive phases of the reference set within the multivariate space defined by CV1 and CV2, axes which account for 95.1% of the total variance (Fig. 6). Separation is driven primarily by variation, in descending order, in the weight percent abundance of CaO, MgO, FeO, and Na_2O (Table 2). Discriminant analysis correctly classifies individual analyses of tephra within the reference set to their volcanic source defined *a priori* approximately 97% of the time (Reference set 1 of Table 3). Misclassifications within the reference set arise primarily amongst the subset of Hasan Dağ eruptives compositionally similar to those from Erciyes Dağ, and between Göllü Dağ and the Acigöl post-caldera eruptive phase. The very good separation along the canonical axes and the high proportion of correctly classified samples among the reference set provides substantial confidence in the use of these data as a classificatory model for tephra of unknown source.

4.2. Attribution of tephra-fall deposits to volcanic source

The tephra-fall samples include previously published analyses by Mouralis (samples R1–R6 from Kaletepe Deresi 3; Slimak et al., 2008) and additional analyses by Tryon and Logan (each with a CAT- prefix) reported here for the first time on replicate samples of R4–R6, and one sample from Körkuyu. All are rhyolitic except for trachytic tephra R6, which because of its composition is not used in the multivariate analyses. Using sample means (Table 1), all five closely superimposed rhyolitic tephra from near the top of and adjacent to the KD3 excavations are attributed to Acigöl (Fig. 6). Tephra R1, R2, R4, and R5 (samples C2D8-R1, C3D4-R2, C2D12-R4, and C3D8-R5) are all attributed to the Acigöl syn-caldera eruptive phase with a ≥99% posterior probability (Table 4) and all occur within the multivariate space defined by the first and second canonical axes for that eruptive phase (Fig. 6). Samples CAT06-42T (=R5) and CAT06-43T (=R4) are similarly

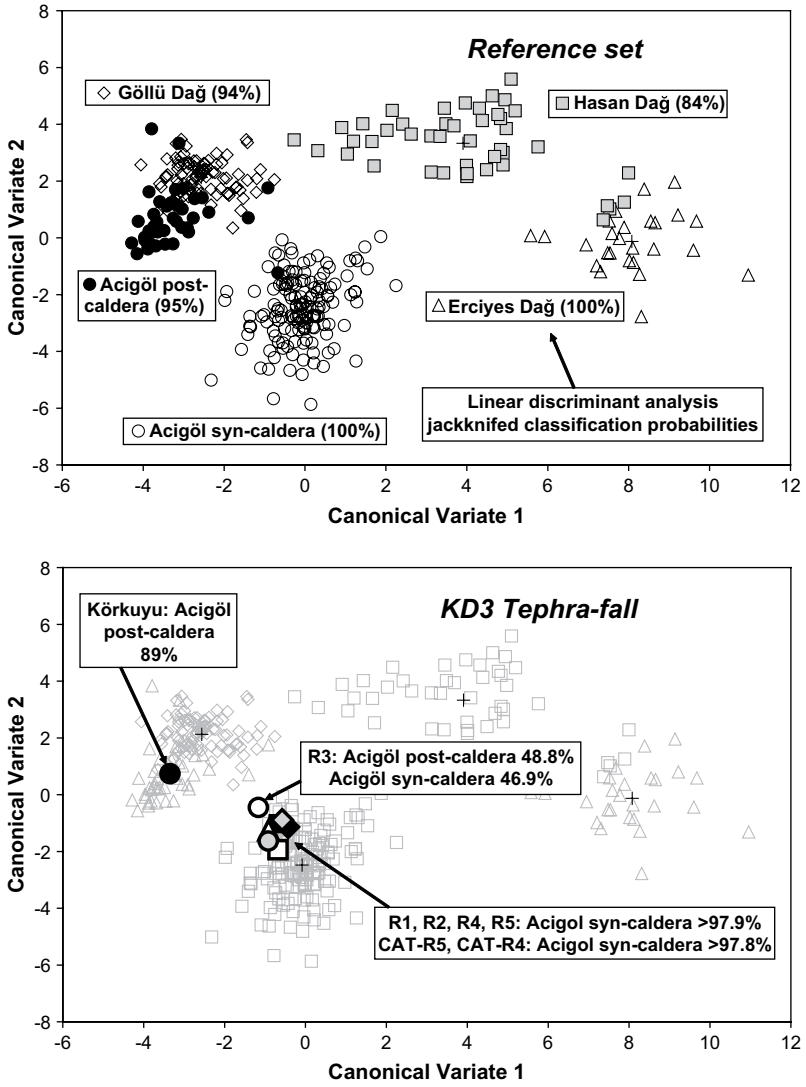

Fig. 6. Plots of the first and second canonical axes for the reference set (upper plot) and airfall tephra from Kaletepe Deresi 3 (lower plot), also showing jackknifed posterior probabilities of classification. Group centroids are marked with a cross.

attributed to the Acigöl syn-caldera eruptive phase using discriminant analysis with a ≥99% posterior probability (Table 4). Tephra R3 most likely derives from Acigöl, although attribution to eruptive phase is not straightforward; inspection of grain-discrete data suggests that the sample consists of multiple compositionally distinct populations, possibly indicating heterogeneous magmas during eruption (cf., Shane et al., 2008). The sample from Körkuyu is classified as deriving from the Acigöl post-caldera eruptive phase, plots within the multivariate space defined by this source, and has a posterior probability of classification of 89% (Fig. 6; Table 4). If this source attribution is correct, the artifacts from this location may be younger than those from Kaletepe Deresi 3.

Our attribution of tephra R1–R5 to an Acigöl source using multivariate statistics provide a complementary approach to prior correlations made on the basis of bivariate plots of normalized abundances in weight percent of SiO_2 and CaO (Mouralis et al., 2002; Mouralis, 2003; Slimak et al., 2004, 2008). Importantly, our classificatory model also attributes replicate analyses of samples R4 and R5 to the same source, with comparable posterior probabilities and similar positions in multivariate space (Fig. 6). These samples (CAT06-42T and CAT06-43T) were analyzed in different laboratories, on different instruments, using different analytical protocols, with marginally different element oxide abundances, that in the case of SiO_2 and Al_2O_3, have means that do not overlap at one standard deviation (Table 1). However, neither SiO_2 nor Al_2O_3 play an important role in distinguishing sources in the multivariate analysis (Table 2). Our classificatory results suggest that the model generated by the analysis of canonical variates and discriminant analysis is robust enough to overcome any errors of precision within our dataset arising from inter-laboratory variation (see also Charman and Grattan, 1999: 148–149; Hunt and Hill, 1996).

Table 2
Correlations between element oxide abundance (in wt. %) for the first two canonical axes of the reference set indicated by the pooled-within canonical structure.

	SiO_2	TiO_2	Al_2O_3	FeO*	MnO	MgO	CaO	Na_2O	K_2O
Reference set									
Canonical variate 1	0.01	0.23	0.25	0.33	−0.06	**0.57**	**0.87**	−0.21	−0.32
Canonical variate 2	0.24	0.12	−0.34	**−0.44**	0.03	0.03	**−0.37**	**−0.39**	−0.04
Reference set + obsidian									
Canonical variate 1	−0.02	0.23	0.24	0.33	−0.06	**0.57**	**0.87**	−0.21	−0.31
Canonical variate 2	0.25	0.12	−0.33	**−0.43**	0.03	0.03	**−0.36**	**−0.39**	−0.05

Variables that best explain observed variation along each axis are shown in bold.
*Total Fe expressed as FeO.

Table 3
Jackknifed classification matrix of volcanic sources and eruptive phases used in the linear discriminant analysis of the two reference sets used in this paper, based on untransformed abundances (in wt. %) of all elements. The last column lists the percent correctly classified to volcanic source defined *a priori* and is thus an estimate of the strength of the classificatory model. NA = not applicable.

	Acigöl post-caldera	Acigöl syn-caldera	Erciyes Dağ	Göllü Dağ	Hasan Dağ	Obsidian	% Correctly classified to known source
Reference set 1: Quaternary volcaniclastics							
Acigöl post-caldera	40	1	0	2	0	NA	93
Acigöl syn-caldera	0	145	0	0	0	NA	100
Erciyes Dağ	0	0	26	0	0	NA	100
Göllü Dağ	2	0	0	87	0	NA	98
Hasan Dağ	0	0	5	2	37	NA	84
Total	42	146	31	91	37	NA	97
Reference set 2: Quaternary volcaniclastics + obsidian							
Acigöl post-caldera	38	1	0	2	0	2	88
Acigöl syn-caldera	0	145	0	0	0	0	100
Erciyes Dağ	0	0	26	0	0	0	100
Göllü Dağ	2	0	0	87	0	0	98
Hasan Dağ	0	0	5	2	37	0	84
Obsidian	5	0	0	0	0	7	58
Total	45	146	31	91	37	9	95

4.3. Compositional variation among the Kaletepe Deresi 3 (KD3) sediments

In the analysis of the KD3 sediments, our objective is to attribute individual pyroclasts to volcanic source where possible and to attempt to identify stratigraphically coherent (but reworked) tephra deposits not observable in outcrop, similar to the use of 'microtephra' or 'cryptotephra' elsewhere (e.g., Alloway et al., 2007; Turney and Lowe, 2001). The total-alkali-silica diagram (Fig. 7) shows three major compositional groups among the analyzed grains from sediments at KD3. Rhyolitic grains are numerically dominant, with lesser amounts of those with intermediate (andesitic–trachytic) and more basic (basaltic–andesitic) compositions. The classification of the rhyolitic grains is treated separately below. The elemental compositions of the intermediate and basic glasses are summarized in Table 5, with a stratigraphic summary provided in Table 6 (see also Fig. 3). The intermediate shards are limited to upper portions of the stratigraphic sequence at KD3 (samples CAT06-24T, -25T, -27, -28T, -38T, and -39T). This stratigraphic position plus their compositional similarity to the R6 tephra (Table 1) exposed in outcrop adjacent to the excavation suggests that these are reworked grains from that deposit. The phenocryst-rich basic glasses (Fig. 4c) present within samples CAT06-21-23T and CAT-34T-37T (Table 6) show wide compositional variability (Table 5), and there is insufficient evidence to support the hypothesis that these grains represent reworked portions of a single eruptive event. However, they are stratigraphically constrained to the middle part of the KD3 excavations (Table 6; Fig. 3), and thus may signal a period of a number of eruptions of basaltic tephra from monogenetic sources or from compositionally diverse batches of magma (e.g., Shane et al., 2008). Basaltic volcanism in the CAVP spans the Early Pleistocene to the Holocene and includes numerous cinder cones and maars that dispersed scoria across a relatively small region (<100 km^2). No correlations among the basaltic tephra are proposed here because of (1) the difficulties associated with comparing the results of EPMA of glass with published whole-rock analyses of lava using X-ray fluorescence, and (2) the continuous range of geochemical compositional variation among the CAVP basalts and thus the lack of diagnostic criteria needed for source identification (Keller, 1974; Ercan et al., 1987, 1990; Olanca, 1994; Druitt et al., 1995; Notsu et al., 1995; Toprak, 1998; Gevrek and Kazanci, 2000; see also Platz et al., 2007; Shane and Smith, 2000).

4.4. Attribution to source of reworked rhyolitic tephra from KD3

As noted above, the classification of rhyolitic glasses from the KD3 sediments used a reference set expanded to include a small sample of locally collected obsidian clasts (reference set 2 of Table 3) broadly similar in composition to the 96 analyses of Göllü Dağ obsidian summarized by Poidevin (1998). The resulting model shows reduced separation among tephra from Göllü Dağ and the Acigöl post-caldera eruptive phase (Fig. 8, upper plot), both of which are similar to the analyzed obsidian clasts. The model including obsidian has a slightly lower posterior probability of correctly attributing grains to their correct source than that used for the tephra-fall deposits (Table 3). However, this model likely reflects a more accurate representation of possible sources of glass within the KD3 sediments, because inclusion of obsidian into the reference set reduced the number of attributions of grains to the Acigöl post-caldera eruptive phase. The presence of *in situ* tephra-fall deposits from the Acigöl syn-caldera eruptive phase near the top of the KD3 excavations suggests that any grains attributed to the later post-caldera collapse eruptions at Acigöl are likely misclassifications on stratigraphic grounds.

All rhyolitic grains with a $\geq$95% posterior probability of classification to one of the six eruptive sources or phases of the reference set (including obsidian) are listed in Table 5, and their positions relative to the first and second canonical variate axes are plotted in Fig. 8. The first and second axes explain 93.4% of the variance among the volcanic sources and eruptive phases of the reference set used in this classification. The stratigraphic positions of these grains from KD3 are summarized in Table 6. The canonical variates plot of the KD3 reworked tephra (Fig. 8, lower plot) suggests three groups useful for the purposes of discussion. The first group (a) includes nine samples (CAT06-24-28T and CAT06-36-39T) that

Table 4
Canonical variate scores (CV1 and CV2) and discriminant analysis results of tephra-fall deposits from Kaletepe Deresi 3 (R1–R5) and Körkuyu. Also shown are the attributed source, Mahalanobis distance (D^2), and posterior probability of classification of each sample. Analyses are based on sample means listed in Table 1.

Sample	CV1	CV2	Attributed source	D^2 to attributed source	Posterior probability of classification to attributed source
Tephra-fall deposits					
C3D8 - R5	−0.7	−1.9	Acigöl syn-caldera	2.4	1.00
CAT06-42T = R5	−0.9	−1.6	Acigöl syn-caldera	2.9	1.00
C2D12 - R4	−0.4	−1.1	Acigöl syn-caldera	3.2	1.00
CAT06-43T = R4	−0.7	−1.0	Acigöl syn-caldera	4.1	0.99
C2D11 - R3	−1.2	−0.4	Acigöl post-/ syn-caldera	8.7/8.8	0.23/0.73
C3D4 - R2	−0.6	−0.9	Acigöl syn-caldera	4.8	0.99
C2D8 - R1	−0.9	−1.2	Acigöl syn-caldera	4.3	0.99
CAT06-46T (Körkuyu)	−3.3	0.7	Acigöl post-caldera	1.3	0.89

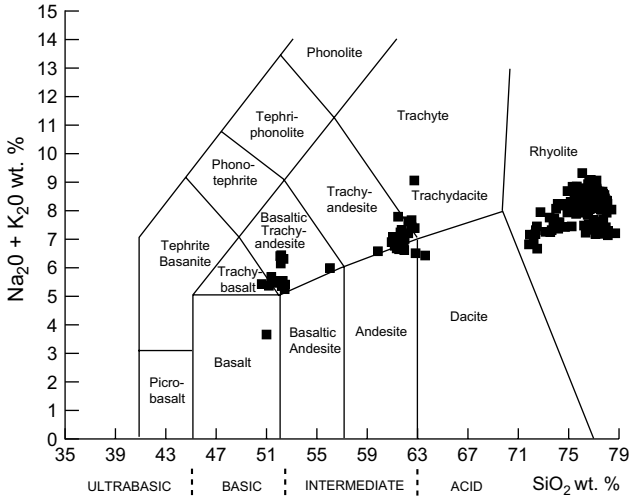

Fig. 7. Normalized values of all vitric grains from Kaletepe Deresi 3 sediments plotted on the total-alkali-silica diagram of Le Bas et al. (1986), showing three broad compositional groups.

contain glasses attributed to the syn-caldera eruptive phases on Acigöl (Table 5, Fig. 8 lower plot). The position of these samples high in the KD3 stratigraphic sequence (Table 6; Fig. 3) strongly suggests that these are reworked portions of the adjacent tephra-fall deposits R1–R5 discussed above, an unsurprising result given previous field correlations of these strata and the clear presence of an incised lapilli-filled stream channel within the upper portions of the *Amont* excavation at KD3 (Slimak et al., 2004; Figs. 2 and 3). The second group (b), shown in the lower plot of Fig. 8 includes grains that have compositions suggesting derivation from Göllü Dağ or the post-caldera eruptions at Acigöl. The latter may represent misclassification or downward migration through bioturbation or other disturbance events, and no grains from this group have much utility for the identification of distal tephra at KD3. The third group (c) shown in the lower plot of Fig. 8 includes grains attributed to Hasan Dağ; these are discussed in greater detail below. No glasses from KD3 are attributed to Erciyes Dağ, >120 km to the east (Fig. 1b), in the opposite direction of the prevailing wind direction today, nor are any attributed on the basis of geochemical composition to local obsidian sources upstream.

4.5. Hasan Dağ correlatives at Kaletepe Deresi 3

Nineteen frequently pumiceous volcaniclastic fragments from nine samples were classified with ≥95% posterior probability as deriving from Hasan Dağ, shown as group (c) in the lower plot of Fig. 8. With the exception of a shard each from CAT06-27T and CAT06-40T, all derive from a single, broad (~2 m) stratigraphic interval near the base of both parallel excavations sampled at KD3 (Tables 5 and 6, Figs. 2 and 3), and many (but not all) plot within the multivariate space defined by the first and second canonical axes for Hasan Dağ. Although defined on the basis of glass geochemical composition, as shown in Fig. 4d this shard population is further distinguished by the presence of relatively large (~400 μm) pyroxene phenocrysts (± smaller Fe–Ti oxides), a typical feature of Hasan Dağ tephra (Mouralis, 2003), but markedly different from the >1000 grains examined from KD3, the great majority of which lacked phenocrysts. The pyroxenes from these glass shards include both calcium-rich clinopyroxne augite (~$Wo_{25}En_{53}Fs_{22}$) as well as orthopyroxene (~$Wo_2En_{68}Fs_{30}$) variants, with the compositional range determined by 27 microprobe analyses on 13 phenocrysts. We provisionally term this population of volcanic glasses the 'KD3 pyroxene tephra' under the assumption that it represents the reworked products of a single tephra-fall event. Initial recognition of Hasan Dağ correlatives was based on eight glass shards (Table 5), followed by 39 microprobe analyses that targeted 11 additional pyroxene-bearing glass shards subsequently attributed to Hasan Dağ with a ≥95% posterior probability of classification. These additional shards are from samples CAT06-31T, -32T, -33T and CAT06-20-21T (Table 5). The combined summary value for the 'KD3 pyroxene tephra' is reported in Table 1 in order to provide a more robust estimate of the geochemical composition of this glass shard population attributed to Hasan Dağ. Mouralis (2003) reported four additional distal tephra deposits from the Göllü Dağ volcanic complex attributed to Hasan Dağ on the basis of geochemical and petrographic similarity. These samples have ~0.28 wt. % TiO_2, twice the amount as the 'KD3 pyroxne tephra' (Table 1), and are thus interpreted as non-correlative distal deposits from different eruptions on Hasan Dağ, which lies > 20 km away (Fig. 1b).

Although we have primarily aimed at attributing tephra to likely volcanic source, additional evidence from Hasan Dağ may provide further chronological control for the archaeological strata at KD3. The presence of both clino- and orthopyroxene phenocrysts in samples of the 'KD3 pyroxene tephra' suggests derivation from earlier eruptive phases of Hasan Dağ. Field stratigraphic and satellite image-based mapping studies suggest three successive stages of edifice construction at the >350 km^3 stratovolcano Hasan Dağ beginning ~7.2 Ma. These are termed the paleo-, meso- and neovolcano by Aydar and Gourgaud (1998), although this nomenclature is not shared among all researchers and reconciliation of individual datasets is not always possible. Most research has focused on the mesovolcano and neovolcano due to the very limited exposure of paleovolcano material because of burial and removal of deposits with subsequent eruptions and lava effusion (and this limited sampling may explain the only partial overlap of KD3 samples with the reference set in Fig. 8). Age estimates for the meso- and neovolcano range from 0.4 Ma to within the last few thousand years (Olanca, 1994; Notsu et al., 1995; Kuzucuoglu et al., 1998), and an image of one of these eruptions may be preserved as part of a painted mural at the Neolithic site of Çatalhöyük (Hodder, 2006; Mellaart, 1967). A single unpublished $^{40}Ar/^{39}Ar$ date of ~6.3 Ma (Arnaud in Deniel et al., 1998: 277) suggests at least one Miocene-aged explosive eruption during the paleovolcano phase. The presence of both clino- and orthopyroxene phenocrysts within the 'KD3 pyroxene tephra' is consistent with derivation from Hasan Dağ paleovolcano eruptions. In the most detailed published geochemical and petrographic analysis of Hasan Dağ, Deniel et al. (1998: 284) noted that *both* clino- and orthopyroxene phenocrysts occur *only* within rhyolitic lavas of the paleovolcano phase. As seen in Fig. 4d, both the clino- and orthopyroxene phenocrysts are in equilibrium with the glass in these samples from KD3, and are thus unlikely to be xenocrysts sampled from underlying rocks.

If we are correct in attributing the 'KD3 pyroxene tephra' to the paleovolcano phase of Hasan Dağ, then glass grains attributed to this deposit have an *eruptive age* of ~6.3–0.4 Ma. However, because the grains attributed to the 'KD3 pyroxene tephra' are clearly reworked, the *depositional age* of these sediments (following the terminology of Feibel et al., 1989: 599–601) and the artifacts they contain are necessarily younger. The depositional age is constrained only by the <1.10 Ma K–Ar estimate of the underlying bedrock and the ~0.16 Ma estimate for overlying tephra-fall deposits R1–R6 at Kaletepe Deresi 3. At present, further age estimates for this deposit remain speculative although important, as the Acheulian biface and cleaver-bearing strata at Kaletepe Deresi 3 (archaeological levels IV–X in Fig. 3) occur within and below glass shards attributed to this deposit. Although dispersed throughout the basal ~2 m of sediments exposed at both the *Amont* and *Aval* sections, the position of the 'KD3 pyroxene tephra' grains low in the stratigraphic sequence makes an Early Pleistocene age for these

Table 5
Summary data for all basic and intermediate grains from the Kaletepe Deresi 3 excavation, divided by compositional group (as determined by position on the total-alkali-silica diagram), as well as all rhyolitic tephra with a ≥95% posterior probability of classification to source, divided by volcanic source. Grain number is preceded by sample number CAT06-XXT. Listed for each grain is the average percent element oxide abundance (wt. %).

Sample/grain	SiO_2	TiO_2	Al_2O_3	FeO*	MnO	MgO	CaO	Na_2O	K_2O	Total	CV1	CV2	D^2 to classified source	Posterior probability of classification
Basaltic–andesitic tephra														
CAT06-37T-2	51.90	1.97	15.73	10.52	0.20	5.28	8.70	4.25	1.28	99.85				
CAT06-37T-12	52.34	1.92	16.70	9.72	0.15	5.28	8.76	4.18	1.20	100.26				
CAT06-36T-11	51.42	2.52	15.45	10.04	0.23	4.32	8.60	3.77	2.29	98.65				
CAT06-35T-2	49.37	1.79	16.01	10.52	0.17	5.60	8.76	4.12	1.17	97.52				
CAT06-35T-10	50.32	2.60	14.70	11.12	0.18	3.66	7.81	3.89	2.30	96.60				
CAT06-35T-8	50.54	1.83	16.28	9.99	0.13	5.74	8.92	4.09	1.21	98.74				
CAT06-34T-1	50.44	1.86	16.58	9.05	0.17	5.53	8.95	3.86	1.71	98.18				
CAT06-23T-3	52.29	1.98	16.68	9.88	0.21	5.56	8.67	4.30	1.25	100.83				
CAT06-23T-4	52.44	2.33	15.46	11.73	0.18	4.83	8.69	4.00	1.25	100.94				
CAT06-22T-15	50.35	3.97	12.49	13.68	0.24	5.18	9.18	2.77	0.85	98.73				
CAT06-22T-10	51.90	2.00	16.29	9.08	0.15	4.97	8.48	4.34	1.91	99.13				
CAT06-22T-6	50.19	2.67	15.00	10.55	0.25	3.67	7.66	3.92	2.28	96.20				
CAT06-21T-1	47.45	1.44	15.63	8.78	0.14	6.26	7.47	4.01	1.03	92.20				
CAT06-21T-9	50.14	2.27	14.61	10.38	0.19	4.60	8.18	3.88	1.30	95.56				
Andesitic–trachytic tephra														
CAT06-39T-18	57.24	1.38	14.45	6.12	0.12	1.61	3.83	4.35	2.45	91.54				
CAT06-39T-5	58.02	1.12	16.83	5.14	0.08	1.86	5.23	4.31	2.01	94.60				
CAT06-39T-8	58.36	1.07	17.50	5.17	0.12	1.53	5.39	4.41	2.19	95.76				
CAT06-39T-3	58.80	0.93	19.69	4.60	0.08	1.34	6.35	4.75	1.71	98.25				
CAT06-39T-20	59.97	1.09	17.56	5.20	0.11	1.75	5.40	4.91	1.93	97.94				
CAT06-39T-2	60.01	1.23	16.84	6.21	0.09	2.08	4.95	4.27	2.37	98.08				
CAT06-39T-10	60.75	1.15	17.29	5.69	0.11	2.01	5.16	4.44	2.12	98.72				
CAT06-39T-6	61.14	1.59	15.17	6.60	0.13	1.90	4.42	3.65	2.69	97.30				
CAT06-38T-11	62.20	1.82	14.50	7.48	0.04	1.64	3.83	3.63	2.66	97.80				
CAT06-28T-4	62.52	1.77	13.73	7.05	0.12	1.71	3.77	4.15	3.52	98.35				
CAT06-27T-10	62.74	1.82	13.92	6.25	0.14	1.36	2.53	4.04	5.02	97.83				
CAT06-25T-7	60.15	1.13	16.86	5.40	0.13	1.70	4.89	4.48	2.32	97.07				
CAT06-24T-11	58.27	1.93	13.79	7.05	0.09	2.02	4.30	4.42	2.97	94.83				
Rhyolitic tephra														
Hasan Dağ														
CAT06-40T-5	73.05	0.16	12.66	1.06	0.03	0.21	1.02	3.68	3.50	95.38	4.30	0.35	15.24	0.98
CAT06-34T-15**	73.22	0.19	12.28	1.03	0.05	0.23	1.11	3.27	3.54	94.94	5.74	2.10	10.96	0.97
CAT06-33-10T	75.98	0.15	12.29	1.23	−0.01	0.15	0.75	3.32	4.14	97.99	1.75	1.88	19.49	1.00
CAT06-33T-20**	73.51	0.12	11.99	1.17	0.05	0.14	0.90	3.32	3.78	94.96	2.83	1.54	14.49	1.00
CAT06-33T-11	75.03	0.16	12.20	0.83	0.03	0.15	0.80	3.08	3.78	96.06	2.67	3.45	4.51	1.00
CAT06-32T-9	71.55	0.11	11.97	1.04	0.04	0.15	0.83	3.13	3.83	92.63	2.22	1.20	14.03	0.97
CAT06-32T-4**	72.92	0.13	11.98	0.87	0.06	0.11	0.91	3.25	3.68	93.93	2.83	2.16	12.95	1.00
CAT06-32T-18**	73.72	0.12	11.90	0.80	0.03	0.13	0.93	3.50	3.72	94.86	3.28	2.67	12.89	1.00
CAT06-32T-14**	74.95	0.13	12.06	0.75	0.09	0.14	0.82	3.26	3.74	95.93	2.64	3.56	8.75	1.00
CAT06-31T-1	74.14	0.15	11.73	0.59	0.03	0.11	0.67	2.66	4.13	94.20	1.43	4.77	13.72	1.00
CAT06-31T-6	71.83	0.14	12.19	0.96	0.08	0.16	1.00	3.40	3.59	93.34	3.74	1.00	14.86	1.00
CAT06-31T-3	72.94	0.13	11.92	1.18	−0.01	0.13	0.89	3.00	3.76	93.94	2.88	1.83	14.83	1.00
CAT06-31T-19**	73.55	0.16	11.96	0.62	0.03	0.11	0.91	3.20	3.80	94.36	3.16	3.32	15.42	1.00
CAT06-27T-13	75.24	0.15	12.85	0.86	0.04	0.18	0.92	3.71	3.73	97.70	3.31	1.23	12.78	1.00
CAT06-23T-2b	73.82	0.14	12.51	0.86	0.07	0.18	0.95	3.65	3.72	95.89	3.51	1.29	12.46	1.00
CAT06-23T-2**	76.42	0.16	12.31	0.88	0.04	0.15	0.88	3.30	4.03	98.16	3.16	3.18	6.74	1.00
CAT06-21T-3	72.43	0.14	11.75	0.87	0.05	0.15	0.88	3.43	3.61	93.32	3.03	2.53	11.65	1.00
CAT06-20T-2	74.93	0.18	12.87	0.92	0.03	0.19	1.02	3.91	3.82	97.87	4.06	0.57	16.56	1.00
CAT06-20T-1**	73.98	0.16	11.79	1.11	0.04	0.16	0.91	3.31	3.94	95.41	3.34	2.51	12.01	1.00
CAT06-33T-2a†	72.50	0.16	12.53	1.13	0.03	0.20	0.81	2.84	3.83	94.03	2.62	1.06	11.83	0.99
CAT06-32T-1a†	71.85	0.18	12.16	1.11	0.03	0.17	1.06	3.02	3.80	93.40	4.49	1.14	11.73	1.00
CAT06-31T-2a**†	74.27	0.14	12.05	0.91	0.03	0.10	0.92	3.74	3.86	96.04	2.63	1.70	17.11	1.00
CAT06-32T-2a**†	72.40	0.13	11.72	0.85	0.05	0.12	0.87	3.53	3.79	93.47	2.47	2.10	15.07	1.00
CAT06-21T-1a†	73.79	0.18	12.12	1.08	0.02	0.17	1.02	3.73	3.86	96.00	4.07	1.30	14.01	1.00
CAT06-20T-2a**†	73.16	0.15	11.70	1.08	0.04	0.15	0.83	3.42	3.84	94.40	2.50	2.25	13.08	1.00
CAT06-33T-5a**†	72.36	0.14	11.81	0.93	0.06	0.15	0.92	3.50	3.68	93.56	3.19	1.98	12.45	1.00
CAT06-32T-3a**†	73.54	0.15	12.05	0.96	0.06	0.15	0.90	3.39	3.86	95.05	3.01	1.99	8.34	1.00
CAT06-33T-4a**†	73.65	0.12	12.06	0.90	0.02	0.15	0.92	3.52	3.80	95.16	3.19	1.99	10.08	1.00
CAT06-33T-1a**†	72.22	0.14	11.86	0.93	0.01	0.15	0.90	3.22	3.69	93.12	3.19	2.21	9.96	1.00
CAT06-32T-4a**†	76.22	0.14	11.96	1.22	0.07	0.15	0.88	3.57	3.91	98.13	2.94	2.54	23.12	1.00
Göllü Dağ														
CAT06-38T-8	73.03	0.07	11.82	0.93	0.06	0.04	0.59	3.31	4.72	94.56	−1.33	0.80	8.02	0.97
CAT06-37T-6	74.52	0.06	12.08	0.97	0.05	0.03	0.45	3.08	5.07	96.31	−2.67	0.85	9.62	0.97
CAT06-35T-18	73.89	0.09	12.21	1.04	0.00	0.03	0.48	3.00	4.30	95.04	−1.97	1.01	9.60	0.97
CAT06-34T-12	72.55	0.03	12.19	0.61	0.03	0.02	0.43	2.84	5.40	94.10	−3.15	0.46	10.54	1.00
CAT06-34T-4	73.14	0.04	12.22	0.67	0.08	0.02	0.46	2.61	6.05	95.28	−3.21	0.19	20.68	1.00
CAT06-33T-18	75.21	0.06	12.39	0.76	0.06	0.03	0.50	3.06	5.60	97.65	−2.51	0.58	12.37	0.96
CAT06-33T-13	73.06	0.06	12.20	0.80	0.11	0.02	0.41	2.77	5.32	94.76	−3.35	0.42	8.00	1.00
CAT06-32T-8	73.58	0.08	12.46	0.43	0.01	0.03	0.42	3.10	5.40	95.50	−3.03	0.78	17.18	0.97
CAT06-29T-1	71.99	0.05	11.53	0.70	0.07	0.03	0.45	3.49	4.21	92.52	−2.28	1.79	4.50	0.96

Table 5 (*continued*)

Sample/grain	SiO_2	TiO_2	Al_2O_3	FeO*	MnO	MgO	CaO	Na_2O	K_2O	Total	CV1	CV2	D^2 to classified source	Posterior probability of classification
CAT06-27T-11	76.35	0.07	12.58	0.51	0.03	0.03	0.52	2.77	4.46	97.32	−1.17	3.11	11.38	0.98
CAT06-26T-11	71.82	0.05	12.15	0.62	0.03	0.06	0.49	3.32	4.60	93.15	−2.04	0.54	8.42	0.95
CAT06-25T-11	74.17	0.06	12.49	0.45	0.04	0.01	0.44	2.77	5.57	96.01	−3.02	1.06	15.42	0.99
CAT06-24T-2	71.04	0.08	12.09	0.84	0.04	0.04	0.53	2.24	6.47	93.37	−2.70	−0.81	42.70	0.96
CAT06-22T-12	72.47	0.06	12.00	0.74	0.04	0.03	0.44	3.25	5.10	94.15	−2.95	0.34	5.13	0.97
CAT06-21T-6	72.60	0.08	12.04	0.67	0.06	0.07	0.63	3.33	4.29	93.77	−0.41	1.44	8.11	0.98
CAT06-19T-4	72.74	0.08	11.93	0.82	0.01	0.02	0.43	3.27	4.99	94.30	−2.98	0.51	5.73	0.97
CAT06-19T-9	72.38	0.05	11.97	0.77	0.04	0.02	0.46	2.81	5.47	93.97	−2.92	0.42	9.48	1.00
CAT06-18T-7	71.01	0.05	11.93	0.76	0.04	0.03	0.48	2.56	5.73	92.60	−2.85	−0.06	17.85	1.00
Acigöl syn-caldera														
CAT06-39T-1	73.10	0.07	12.96	0.87	0.06	0.06	0.69	3.43	4.35	95.58	−0.68	−1.29	4.88	1.00
CAT06-39T-11	73.81	0.07	13.03	1.05	0.02	0.06	0.72	3.68	4.44	96.87	−0.62	−2.05	2.05	1.00
CAT06-39T-19	72.81	0.07	12.85	0.90	0.13	0.06	0.86	3.44	4.33	95.42	0.65	−1.39	7.64	1.00
CAT06-39T-15	72.47	0.07	13.01	0.99	0.09	0.06	0.75	3.63	4.27	95.35	−0.48	−2.33	2.30	1.00
CAT06-39T-12	72.25	0.08	13.06	1.05	0.03	0.07	0.73	3.80	4.05	95.12	−0.49	−2.64	2.68	1.00
CAT06-39T-17	71.70	0.07	12.91	1.06	0.06	0.06	0.74	3.71	4.10	94.41	−0.56	−2.65	2.44	1.00
CAT06-39T-7	72.50	0.08	12.90	1.18	0.15	0.08	0.75	3.76	4.20	95.59	−0.43	−2.60	3.95	1.00
CAT06-39T-13	73.21	0.09	13.41	1.33	0.06	0.09	0.73	3.84	4.19	96.95	−0.66	−3.79	5.30	1.00
CAT06-38T-17	73.78	0.06	12.50	0.92	0.02	0.05	0.71	3.85	4.38	96.28	−0.51	−0.75	6.87	0.97
CAT06-38T-7	73.72	0.07	12.72	0.86	0.00	0.06	0.71	3.67	4.22	96.03	−0.25	−0.58	7.62	0.98
CAT06-38T-14	75.12	0.05	12.79	0.99	0.04	0.06	0.75	3.79	4.54	98.13	−0.19	−0.97	7.22	0.99
CAT06-38T-16	72.98	0.06	12.43	1.04	0.00	0.06	0.70	3.55	4.28	95.10	−0.40	−0.76	6.60	0.99
CAT06-38T-13	72.93	0.10	12.50	1.02	0.07	0.07	0.74	3.78	3.88	95.10	0.12	−0.67	6.91	1.00
CAT06-38T-5	71.20	0.05	12.52	0.95	0.05	0.03	0.80	3.70	4.00	93.30	−0.11	−1.86	8.19	1.00
CAT06-38T-19	74.53	0.09	12.99	1.28	0.07	0.07	0.82	3.76	4.29	97.90	0.31	−2.15	6.83	1.00
CAT06-38T-2	71.27	0.10	12.58	1.03	0.03	0.05	0.80	4.01	4.33	94.20	−0.24	−2.70	3.30	1.00
CAT06-38T-6	72.50	0.10	13.25	1.52	0.04	0.09	0.87	4.25	4.16	96.78	0.22	−4.95	12.50	1.00
CAT06-37T-3	72.93	0.08	12.31	1.00	0.04	0.06	0.73	3.55	4.33	95.04	−0.11	−0.42	7.14	0.99
CAT06-37T-5	74.60	0.08	12.86	1.17	0.02	0.05	0.67	3.91	4.19	97.54	−0.97	−1.66	7.44	1.00
CAT06-36T-7	71.06	0.07	12.77	0.69	0.06	0.05	0.74	3.65	4.11	93.21	−0.41	−1.58	15.85	1.00
CAT06-36T-4	71.74	0.08	12.95	0.82	0.05	0.06	0.72	3.58	4.21	94.21	−0.55	−1.90	8.19	1.00
CAT06-36T-6	72.10	0.07	12.84	0.97	0.03	0.05	0.73	3.60	4.12	94.50	−0.51	−1.92	3.75	1.00
CAT06-36T-16	71.16	0.06	12.91	0.79	0.05	0.05	0.75	3.36	4.35	93.48	−0.46	−2.00	10.84	1.00
CAT06-36T-2	70.23	0.06	12.64	0.93	0.06	0.05	0.72	3.38	4.46	92.52	−0.89	−2.42	6.93	1.00
CAT06-36T-14	71.53	0.08	12.86	0.93	0.03	0.06	0.75	3.62	4.03	93.90	−0.24	−2.01	5.50	1.00
CAT06-36T-5	70.96	0.07	12.93	0.74	0.05	0.05	0.76	3.66	4.38	93.61	−0.54	−2.44	13.17	1.00
CAT06-36T-20	72.39	0.09	13.01	0.95	0.02	0.06	0.76	3.65	4.21	95.14	−0.22	−2.15	3.41	1.00
CAT06-36T-15	71.44	0.08	12.94	1.13	0.07	0.07	0.75	2.81	4.64	93.92	−0.33	−2.24	5.94	1.00
CAT06-36T-3	72.56	0.08	12.94	1.15	0.07	0.06	0.74	3.53	4.20	95.34	−0.48	−2.34	1.65	1.00
CAT06-36T-12	72.55	0.08	13.11	1.12	0.09	0.06	0.71	3.72	4.32	95.75	−1.01	−3.03	2.32	1.00
CAT06-36T-19	71.53	0.08	12.98	1.06	0.10	0.07	0.74	3.68	4.20	94.43	−0.61	−2.88	3.03	1.00
CAT06-36T-17	71.64	0.09	12.93	1.09	0.07	0.05	0.75	3.61	4.29	94.51	−0.67	−2.87	2.33	1.00
CAT06-36T-8	71.31	0.07	12.87	1.09	0.11	0.06	0.76	3.67	4.16	94.11	−0.54	−2.88	3.48	1.00
CAT06-36T-1	71.07	0.07	12.85	1.29	0.02	0.05	0.75	3.75	4.31	94.18	−0.90	−3.85	6.15	1.00
CAT06-28T-2	74.00	0.06	12.63	0.91	0.05	0.06	0.71	3.74	4.33	96.52	−0.39	−0.64	5.77	0.98
CAT06-28T-7	74.13	0.06	12.70	0.92	0.04	0.07	0.74	3.93	4.31	96.91	−0.14	−0.96	5.37	0.99
CAT06-28T-13	73.86	0.08	13.00	1.15	0.07	0.07	0.74	3.82	3.91	96.71	−0.19	−1.83	3.73	1.00
CAT06-27T-12	74.71	0.06	13.21	1.04	0.06	0.06	0.72	3.01	4.42	97.29	−0.28	−1.01	5.79	1.00
CAT06-26T-10	71.88	0.07	12.87	1.02	0.07	0.05	0.74	3.85	4.48	95.04	−0.92	−3.00	2.14	1.00
CAT06-25T-1	72.99	0.08	13.52	0.83	0.03	0.05	0.84	4.20	4.37	96.92	−0.19	−3.72	13.09	1.00
CAT06-24T-7	73.44	0.09	12.68	0.91	0.05	0.05	0.59	3.60	4.79	96.21	−1.77	−1.23	5.84	0.96
CAT06-24T-10	71.65	0.08	12.72	0.87	0.06	0.08	0.74	3.80	4.16	94.18	−0.20	−1.73	5.25	1.00
CAT06-24T-9	72.34	0.06	12.69	1.13	0.10	0.04	0.68	3.76	4.35	95.16	−1.37	−2.47	4.26	1.00
CAT06-24T-5	71.51	0.08	12.77	1.07	0.10	0.07	0.69	4.09	4.28	94.66	−1.20	−3.09	3.56	1.00
CAT06-24T-1	71.33	0.07	12.63	1.03	0.08	0.06	0.75	3.88	4.35	94.17	−0.64	−2.64	2.07	1.00
CAT06-24T-4	71.41	0.09	12.85	1.16	0.06	0.08	0.72	3.93	4.14	94.44	−0.71	−3.12	2.36	1.00
Acigöl post-caldera														
CAT06-22T-11	74.94	0.05	12.57	0.65	0.09	0.02	0.46	4.15	4.37	97.29	−2.89	−0.03	2.07	0.95
CAT06-21T-2	73.67	0.04	12.37	0.50	0.04	0.02	0.44	4.04	4.31	95.44	−2.88	0.40	7.27	0.95

*Total Fe expressed as FeO. Also included for the rhyolitic grains are the canonical scores, Mahalanobis distance (D^2) and posterior probability of classification used in the analysis of canonical variates and discriminant analysis. Note that although all samples attributed to Hasan Dağ have a posterior probability ≥95%, those samples that also fall within the multivariate space defined by the first and second canonical axes of Fig. 8 are denoted with two asterisks (**). Analyses that result from specific targeting of Hasan Dağ correlative grains following initial reconnaissance are marked with a dagger (†).

sediments plausible (defined here as older than the Brunhes–Matuyama polarity reversal at ~0.78 Ma; Sarna-Wojcicki et al., 2000; Singer et al., 2002). The hypothesis of an Early Pleistocene age assumes rapid sedimentation after the eruption of the rhyolite bedrock and a brief interval between the eruption of the tephra and the timing of its deposition as components of a reworked tuffaceous sand at Kaletepe Deresi 3. Testing this hypothesis and increasing the chronological resolution of the age of the Paleolithic artifacts beyond that provided by the bedrock and overlying R1–R6 tephra (~1.10–0.16 Ma) requires paleomagnetic studies of Kaletepe Deresi 3 sediments or similar methods that constrain the timing of tephra *deposition* rather than tephra *eruption* (supplemented where possible by radiometric age estimates of distal or proximal tephra deposits from Hasan Dağ or basaltic sources by K–Ar, $^{40}Ar/^{39}Ar$ or fission-track methods). This lack of further chronological control marks the current limits of our efforts towards constructing a tephra-based stratigraphic framework for the Central Anatolian Volcanic Province.

Table 6
Summary stratigraphic position of all vitric grains from Kaletepe Deresi 3 assigned to source (≥95% posterior probability using linear discriminant analysis for acidic/rhyolitic grains) or compositional type for basic or intermediate grains (as determined by position on the total-alkali-silica diagram). Also shown is the total number of glass shards analyzed (i.e., including those not classified to source with ≥95% posterior probability). Samples are listed in stratigraphic order from the adjacent *Aval* and *Amont* excavations and exposures of tephra-fall deposits R1–R6 adjacent to and upstream from the *Amont* excavation (see Figs. 2 and 3).

Aval

Sample	Count of shards examined	Acigol syn-caldera	Acigol post-caldera	Golludag	Hasandag	Erciyes Dag	Obsidian	Andesite-trachyte	Basalt-andesite
CAT06-29T	13			1					
CAT06-28T	13	3						1	
CAT06-27T	13	1		1	1			1	
CAT06-26T	13	1		1					
CAT06-25T	12	1		1				1	
CAT06-24T	14	6		1				1	
CAT06-23T	11				2				2
CAT06-22T	15		1	1					3
CAT06-21T	10		1	1	1				2
CAT06-20T	6				2				
CAT06-19T	13			2					
CAT06-18T	13			1					
CAT06-17T	13								
Zone		***1***			***3***			***1***	***2***

Amont

Sample	Count of shards examined	Acigol syn-caldera	Acigol post-caldera	Golludag	Hasandag	Erciyes Dag	Obsidian	Andesite-trachyte	Basalt-andesite
CAT06-39T	20	8						8	
CAT06-36T	20	15						1	1
CAT06-38T	19	9		1					
CAT06-37T	12	2		1					2
CAT06-35T	19			1					3
CAT06-34T	15			2	1				1
CAT06-32T	15			1	4				
CAT06-33T	18			2	3				
CAT06-31T	18				4				
CAT06-30T	17								
CAT06-40T	6				1				
Zone		***1***			***3***			***1***	***2***

Tephra-fall deposits R1-R6

Sample	Count of shards examined	Acigol syn-caldera	Acigol post-caldera	Golludag	Hasandag	Erciyes Dag	Obsidian	Andesite-trachyte	Basalt-andesite
R6 (CAT06-41T, C2D14)	29							29	
R5 (CAT06-42T, C3D8)	19	19							
R4 (CAT06-43T, C2D12)	22	22							
R3 (C2D11)	12	7	2	1			2		
R2 (C3D4)	7	6		1					
R1 (C2D8)	17	15	2						
Zone		***1***						***1***	

Boxed cells indicate presence of shards of a particular composition or source; number within denotes shard count for that source. Shard counts likely but do not necessarily indicate relative abundance because of the non-random sampling procedure used here. 'Zone' refers to reworked tephra 'zones' shown in Fig. 9 and discussed in text.

5. Summary and conclusions

Multivariate statistical analyses of major and minor element oxide abundances are used to distinguish among a reference set of proximal tephra deposits from five eruptive phases (and obsidian flows) from four volcanic edifices within the Central Anatolian Volcanic Province (CAVP). Analysis of canonical variates shows excellent separation among the eruptive phases within the reference set, and linear discriminant analysis results in correctly classified samples (as estimated by the cross-validation method) ~95% of the time. This probabilistic classificatory model, based on a reference set of compositionally distinct tephra from known volcanic sources, forms the basis of a tephrostratigraphic framework that we use to classify distal deposits of unknown source. In this study, we have applied this framework to tephra fallout and variably reworked volcaniclastic deposits from the archaeological sites Kaletepe Deresi 3 (KD3) and Körkuyu in an attempt to attribute these deposits to volcanic source or eruptive phase.

Fig. 9 provides a summary of the tephrostratigraphic and archaeological data from KD3 and Körkuyu. The electron microprobe-based 'geochemical reconnaissance' of >330 glass shards from 24 samples of reworked tuffaceous sediments from KD3 (Table 6) suggests the presence of at least three stratigraphic 'zones.' Each 'zone' consists of reworked tephra deposits that are characterized by one or more populations of glass shards compositionally distinct from those found in other 'zones.' 'Reworked tephra zone 1' includes the locally redeposited lateral equivalents of rhyolitic and trachytic airfall tephra previously correlated to Acigöl syn-caldera deposits and Kurugölkabak Tepe, respectively (Mouralis et al., 2002; Slimak et al., 2004, 2008), and consists of Levallois-dominated Middle Paleolithic archaeological assemblages. 'Reworked tephra zone 2' comprises basaltic tephra of unknown source, and contains Middle Paleolithic assemblages that lack evidence for Levallois flake production and also includes biface-bearing Lower Paleolithic assemblages. 'Reworked tephra zone 3' contains the provisionally-termed 'KD3 pyroxene tephra' attributed to the Hasan Dağ paleovolcano, found vertically dispersed only throughout the biface-bearing basal ~2 m of the KD3 excavations. Neither the eruptive nor depositional ages of the 'KD3 pyroxene tephra' are as yet known with certainty, although available techno-typological, chronometric, stratigraphic, and petrographic evidence are consistent with a Middle and possibly an Early Pleistocene age for this deposit. If the latter is verified, Kaletepe Deresi 3 would join 'Ubeidiya, Israel (Verosub and Tchernov, 1991; Bar-Yosef and Goren-Inbar, 1993), possibly Isampur, India (cf., Paddayya et al., 2002; Acharyya, 2003), and localities in the Bose Basin, China (Yamei et al., 2000) as the only sites preserving Early Pleistocene Acheulian assemblages outside of Africa. Importantly, at 1600 m a.s.l. in an area that experiences harsh winters during the present interglacial period, occupation would have been challenging for hominin populations during much of the Pleistocene. KD3 may yet provide important information on the timing of hominin occupation of cold, temperate environments, provided further chronological control is obtained.

The tephra correlations proposed in this study do provide modest constraints on the likely ages of CAVP Middle Paleolithic assemblages at Körkuyu and Kaletepe Deresi 3 (Fig. 9). Tephra-fall deposits from Körkuyu are attributed to post-caldera eruptions from Acigöl that likely date to ~0.07–0.02 Ma (Bigazzi et al., 1993; Druitt et al., 1995), providing maximum ages for the overlying artifacts. Tephra fallout deposits near the summit of the excavations of KD3 have been attributed to syn-caldera eruptions at Acigöl dated to ~0.16 Ma (Mouralis et al., 2002; Slimak et al., 2004, 2008), a finding corroborated here using a complementary correlative methodology. The richest Middle Paleolithic levels at KD3 (Level II of Slimak et al., 2004, 2008) occur below the Acigöl syn-caldera deposits, and are thus >0.16 Ma and stratigraphically overlie the undated 'KD3 pyroxene tephra.' Middle Paleolithic assemblages at

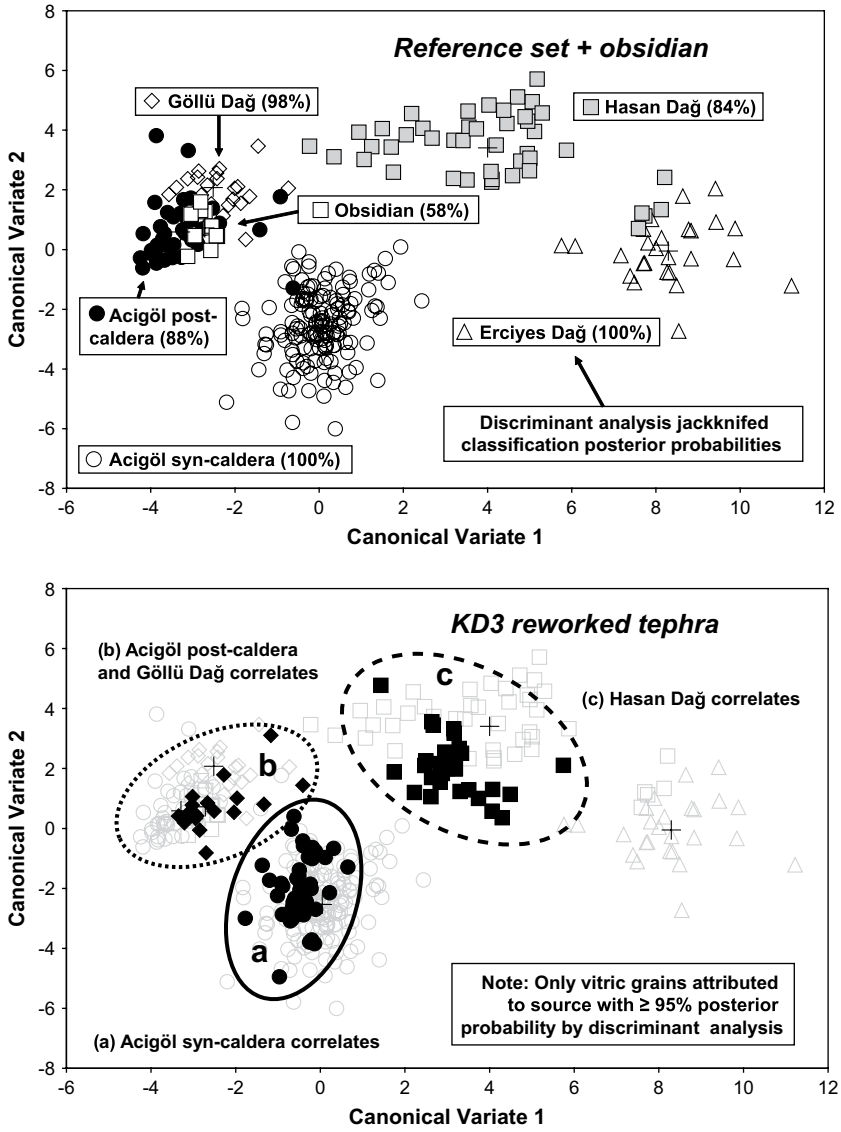

Fig. 8. Plots of the first and second canonical axes for the reference set including obsidian (upper plot) and reworked tephra from Kaletepe Deresi 3 (lower plot). Group centroids are marked with a cross. Note that the lower plot includes only those vitric grains attributed to one of the six components of the reference set with ≥95% posterior probability of classification. Ovals demarcating groups a–c in the lower plot are arbitrary and are used only for the purpose of discussion; see text for details.

Körkuyu and KD3 both show Levallois methods of flake production, but initial inspection suggests substantial inter-assemblage variation. If our source attributions and age estimates are correct, the two assemblages may differ by at least 0.09 Ma, providing further basis for examining temporal trends within the Anatolian Middle Paleolithic.

Our use of canonical variates analysis and discriminant analysis provides a classificatory method that incorporates the full range of geochemical data, provides a probabilistic estimation of source attribution for distal tephra, and is sufficiently robust to incorporate large ($n > 1200$) datasets of geochemical compositional analyses generated by multiple laboratories. Although promising, relative to existing tephrochronological frameworks elsewhere, there remains substantial room for further detailed studies in assessing the range of compositional variation among CAVP eruptives (cf., Shane, 2000; see also Stokes et al., 1992), and particularly chronological constraints on the timing of these tephra-producing events (cf., McDougall and Brown, 2006). Increasing the resolution of CAVP tephra correlation beyond attribution to source or broad eruptive phase to the identification of specific eruptive events and their products will require more extensive sampling of sources and thus an expanded reference set, the use of additional analytical methods, improved means of data comparison, and a refined degree of precision to determine sample equivalence (for examples and further discussion, see Davies et al., 2002; Feibel, 1999; Pearce et al., 2007; Pyle et al., 2006; Sarna-Wojcicki, 2000; Stokes et al., 1992; Turney et al., 2008; see also Shackley, 2008). We note in closing that this project remains in its early stages. However, the recent discovery of additional Paleolithic sites associated with volcaniclastic deposits in the CAVP (Balkan-Atlı et al., 2008), combined with the promising initial results described here (but tempered by the clear need for further radiometric age estimates), suggests the potential for tephrostratigraphy as an essential method in the analysis of archaeological variation in Anatolia, comparable to that already developed for Paleolithic sequences elsewhere in Eurasia and Africa.

Acknowledgements

We thank the Department of Cultural Assets and Museums, Ministry of Tourism and Culture of Turkey for permission to conduct research at Kaletepe, and would like to particularly

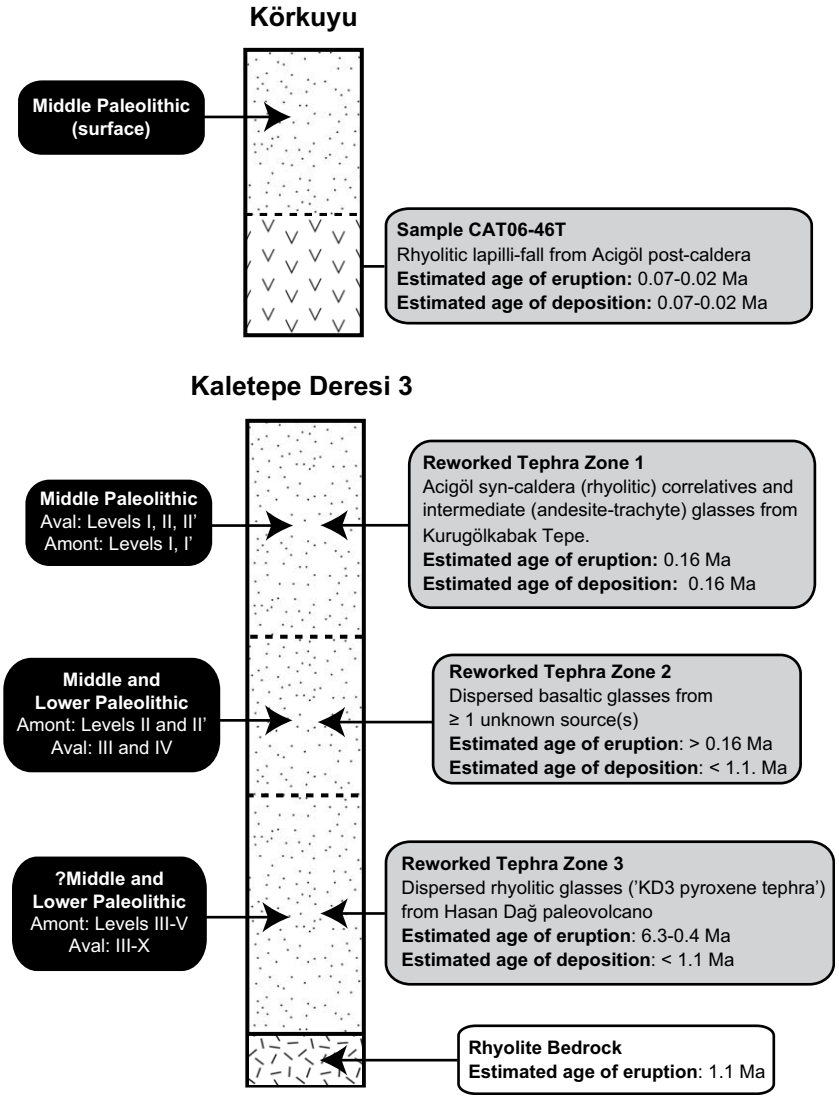

Fig. 9. Summary schematic stratigraphic columns showing relative position and estimated ages of reworked tephra 'zones' and artifacts at sites Kaletepe Deresi 3 and Körkuyu. Zone boundary estimates are limited by ~50-cm resolution of vertical sampling, and there is some overlap; see Table 6 for assignment of individual samples.

acknowledge the assistance and encouragement provided by Dr. Fazil Acikgoz, director of the Nigde Museum. Financial support was provided by grants from the L.S.B. Leakey Foundation to Kuhn and from the Research Fund of Istanbul University (project number 533/05052006) and the French Ministry of Foreign Affairs (la mission de Préhistoire Anatolienne) to Balkan-Atlı. Two anonymous readers provided thorough and very valuable reviews that resulted in a substantially improved manuscript. Finally, support and assistance from Rick Potts, Matt Tocheri, and Rhonda Kauffman are greatly appreciated.

References

Acharyya, S.K., 2003. Recent findings on the Acheulian of Isampur excavations and its dating. Current Science 84, 127–128.

Aitchison, J., 1986. The Statistical Analysis of Compositional Data. Chapman and Hall, London.

Alloway, B.V., Larsen, G., Lowe, D.J., Shane, P.A.R., Westgate, J.A., 2007. Tephrochronology. In: Elias, S.A. (Ed.), Encyclopedia of Quaternary Science. Elsevier, Boston, pp. 2869–2898.

Anikovich, M.V., Sinitsyn, A.A., Hoffecker, J.F., Holliday, V.T., Popov, V.V., Lisitsyn, S.N., Forman, S.L., Leykovskaya, G.M., Pospelova, G.A., Kuz'mina, I.E., Burova, N.D., Goldberg, P., Macphail, R.I., Giacco, B., Praslov, N.D., 2007. Early Upper Paleolithic in eastern Europe and implications for the dispersal of modern humans. Science 315, 223–226.

Aydar, E., Gourgaud, A., 1998. The geology of Mount Hasan stratovolcano, central Anatolia, Turkey. Journal of Volcanology and Geothermal Research 85, 129–152.

Balkan-Atlı, N., Kuhn, S., Astruc, L., Çakan, G., Dinçer, B., Kayacan, N., 2008. Göllü Dağ 2007 survey. Anatolia Antiqua 16, 293–312.

Bar-Yosef, O., Goren-Inbar, N., 1993. The Lithic Assemblages of 'Ubeidiya. In: Monographs of the Institute of Archaeology, Qedem 34. Hebrew University, Jerusalem.

Baxter, M.J., 1994a. Exploratory Multivariate Analysis in Archaeology. Edinburgh University Press, Edinburgh.

Baxter, M.J., 1994b. Stepwise discriminant analysis in archaeometry: a critique. Journal of Archaeological Science 21, 659–666.

Baxter, M.J., Beardah, C.C., Cool, H.E.M., Jackson, C.M., 2005. Compositional data analysis of some alkaline glasses. Mathematical Geology 37, 183–196.

Bigazzi, G., Yeğingil, Z., Ercan, T., Oddone, M., Özdoğan, M., 1993. Fission track dating obsidians in Central and Northern Anatolia. Bulletin of Volcanology 55, 588–595.

Brown, F.H., Haileab, B., McDougall, I., 2006. Sequence of tuffs between the KBS Tuff and the Chari Tuff in the Turkana Basin, Kenya and Ethiopia. Journal of the Geological Society, London 163, 185–204.

Brown, F.H., Sarna-Wojcicki, A.M., Meyer, C.E., Haileab, B., 1992. Correlation of Pliocene and Pleistocene tephra layers between the Turkana Basin of East Africa and the Gulf of Aden. Quaternary International 13/14, 55–67.

Campisano, C.J., Feibel, C.S. Tephrostratigraphy of the Hadar and Busidima Formations at Hadar, Afar Depression, Ethiopia. In: Quade, J., Wynn, J. (Eds.), The Geology of Early Humans in the Horn of Africa. Geological Society of America Special Paper, in press.

Charman, D.J., Grattan, J., 1999. An assessment of discriminant function analysis in the identification and correlation of distal Icelandic tephras in the British Isles. In: Firth, C.R., McGuire, W.J. (Eds.), Volcanoes in the Quaternary. Geological Society London, London, pp. 147–160.

Davies, S.M., Branch, N.P., Lowe, J.J., Turney, C.S.M., 2002. Towards a European tephrochronological framework for Termination 1 and the Early Holocene. Philosophical Transactions of the Royal Society of London A360, 767–802.

Deniel, C., Aydar, E., Gourgaud, A., 1998. The Hasan Dagi stratovolcano (Central Anatolia, Turkey): evolution from calc-alkaline to alkaline magmatism in a collision zone. Journal of Volcanology and Geothermal Research 87, 275–302.

Donovan, J.J., 2006. Probe for Windows User's Guide and Reference. Enterprise edition. Advanced Microbeam, Vienna, OH.

Druitt, T.H., Brenchley, P.J., Gökten, Y.E., Francaviglia, V., 1995. Late Quaternary rhyolitic eruptions from the Acigöl Complex, central Turkey. Journal of the Geological Society, London 152, 655–667.

Ercan, T., Tokel, S., Can, B., Fişekçi, A., Fujitani, T., Notsu, K., Selvi, Y., Ölmez, M., Matsuda, J.I., Ui, T., Yildirim, T., Akbaşli, A., 1990. The origin and evolution of the Cenozoic volcanism of Hasandağı-Karacadağ area (Central Anatolia). Jeomorfoloji Dergïsi 18, 39–54 (in Turkish).

Ercan, T., Yildrim, T., Akbaşli, 1987. Characteristic features of the volcanism between Gelveri (Niğde) and Kizilcin (Nevşehir). Jeomorfoloji Dergïsi 15, 27–36 (in Turkish).

Feibel, C.S., 1999. Tephrostratigraphy and geological context in paleoanthropology. Evolutionary Anthropology 8, 87–100.

Feibel, C.S., Brown, F.H., McDougall, I., 1989. Stratigraphic context of fossil hominids from the Omo Group deposits: Northern Turkana basin, Kenya and Ethiopia. American Journal of Physical Anthropology 78, 595–622.

Froggatt, P.C., 1992. Standardization of the chemical analysis of tephra deposits. Report of the ICCT Working Group. Quaternary International 13/14, 93–96.

Gevrek, A.I., Kazanci, N., 2000. A Pleistocene, pyroclastic-poor maar from central Anatolia, Turkey: influence of a local fault on a phreatomagmatic eruption. Journal of Volcanology and Geothermal Research 95, 309–317.

Hodder, I., 2006. The Leopard's Tale: Revealing the Mysteries of Çatalhöyük. Thames and Hudson, London.

Hunt, J.B., Hill, P.G., 1993. Tephra geochemistry: a discussion of some persistent analytical problems. The Holocene 3, 272–278.

Hunt, J.B., Hill, P.G., 1996. An inter-laboratory comparison of the electron probe microanalysis of glass geochemistry. Quaternary International 34-36, 229–241.

Hunt, J.B., Hill, P.G., 2001. Tephrological implications of beam size-sample size effects in electron microprobe analysis of glass shards. Journal of Quaternary Science 16, 105–117.

Innocenti, F., Mazzuoli, R., Pasquaré, G., Villari, L., 1982. Anatolia and north-western Iran. In: Thorpe, R.S. (Ed.), Andesites. John Wiley and Sons, New York, pp. 327–349.

Jarosewich, E., Nelson, J.A., Norbers, J.A., 1980. Reference samples for electron microprobe analysis. Geostandards Newsletter 4, 43–47.

Johnson, R.A., Wichern, D.W., 2002. Applied Multivariate Statistical Analysis, fifth ed. Prentice Hall, Upper Saddle River, NJ.

Kappelman, J., Alçiçek, M., Kazanci, N., Schultz, M., Özkul, M., Sen, Ş., 2007. Brief communication: first *Homo erectus* from Turkey and implications for migrations into temperate Eurasia. American Journal of Physical Anthropology 135, 110–116.

Keller, J., 1974. Quaternary maar volcanism near Karapinar in Central Anatolia. Bulletin Volcanologique 38, 378–396.

Kuhn, S.L., 2002. Paleolithic archaeology in Turkey. Evolutionary Anthropology 11, 198–210.

Kürkçüoglu, B.E.S., Aydar, E., Gourgaud, A., Gündogdu, N., 1998. Geochemical approach to magmatic evolution of Mt. Erciyes stratovolcano Central Anatolia, Turkey. Journal of Volcanology and Geothermal Research 85, 473–494.

Kuzucuoglu, C., Pastre, J.-F., Black, S., Ercan, T., Fontugne, M., Guillou, H., Hatté, C., Karabiyikoglu, M., Orth, P., Türkecan, A., 1998. Identification and dating of tephra layers from Quaternary sedimentary sequences of Inner Anatolia, Turkey. Journal of Volcanology and Geothermal Research 85, 153–172.

Le Bas, M.J., Le Maitre, R.W., Streckeisen, A., Zanettin, B., 1986. A chemical classification of volcanic rocks based on the total alkali-silica diagram. Journal of Petrology 27, 745–750.

McDougall, I., Brown, F.H., 2006. Precise $^{40}Ar/^{39}Ar$ geochronology for the upper Koobi Fora formation, Turkana Basin, northern Kenya. Journal of the Geological Society, London 163, 205–220.

McHenry, L.J., Mollel, G.F., Swisher, C.C.I., 2008. Compositional and textural correlations between Olduvai Gorge Bed I tephra and volcanic sources in the Ngorongoro Volcanic Highlands, Tanzania. Quaternary International 178, 306–319.

Mellaart, J., 1967. Çatal Hüyük: A Neolithic Town in Anatolia. McGraw-Hill Book Company, New York.

deMenocal, P.B., Brown, F.H., 1999. Pliocene tephra correlations between East African hominid localities, the Gulf of Aden and the Arabian Sea. In: Agusti, J., Rook, L., Andrews, P. (Eds.), The Evolution of Terrestrial Ecosystems in Europe. Cambridge University Press, Cambridge, pp. 23–54.

Mouralis, D., 2003. Les complexes volcaniques quaternarires de Cappadoce (Göllüdağ et Acigöl) – Turquie: Évolutions morphodynamiques et implications environnementales. Thèse de Doctorat, Université Paris 12, Paris.

Mouralis, D., Pastre, J.-F., Kuzucuoğlu, C., Türkecan, A., Atici, Y., Slimak, L., Guillou, H., Kunesch, S., 2002. Les complexes volcaniques rhyolitiques quaternaires d'Anatolie centrale (Göllü Dag et Acigöl, Turquie): Genèse, instabilité, contraintes environnementales. Quaternaire 13, 219–228.

Notsu, K., Fujitani, T., Ui, T., Matsuda, J., Ercan, T., 1995. Geochemical features of collision-related volcanic rocks in central and eastern Anatolia, Turkey. Journal of Volcanology and Geothermal Research 64, 171–192.

Olanca, K., 1994. Geochimie des laves quaternaires de Cappadoce (Turquie): Les appareils monogeniques. Thèse de Doctorat, Université Blaise Pascal, Clermont Ferrand.

Otte, M., Yalçinkaya, I., Kozlowski, J., Bar-Yosef, O., López Bayón, I., Taskiran, H., 1998. Long-term technical evolution and human remains in the Anatolian Palaeolithic. Journal of Human Evolution 34, 413–431.

Paddayya, K., Blackwell, B.A.B., Jhaldiyal, R., Petraglia, M.D., Fevrier, S., Chaderton, D.A.I., Blickstein, J.I.B., Skinner, A.R., 2002. Recent findings on the Acheulian of the Hunsgi and Baichbal valleys, Karnataka, with special reference to the Isampur excavation and its dating. Current Science 83, 641–647.

Pasquarè, G., Poli, S., Vezzoli, L., Zanchi, A., 1988. Continental arc volcanism and tectonic setting in Central Anatolia, Turkey. Tectonophysics 146, 217–230.

Pearce, N.J., Denton, J.S., Perkins, W.T., Westgate, J.A., Alloway, B.V., 2007. Correlation and characterization of individual glass shards from tephra deposits using trace element laser ablation ICP–MS analyses: current status and future potential. Journal of Quaternary Science 22, 721–736.

Pearce, N.J.G., Bendall, C.A., Westgate, J.A., 2008. Comment on "Some numerical considerations in the geochemical analysis of distal microtephra" by A.M. Pollard, S.P.E. Blockley and C.S. Lane. Applied Geochemistry 23, 1353–1364.

Petraglia, M., Korisettar, R., Boivin, N., Clarkson, C., Ditchfield, P., Jones, S., Koshy, J., Lahr, M.M., Oppenheimer, C., Pyle, D., Roberts, R., Schwenninger, J.-L., Arnold, L., White, K., 2007. Middle Paleolithic assemblages from the Indian subcontinent before and after the Toba super-eruption. Science 317, 114–116.

Platz, T., Cronin, S.J., Smith, I.E.M., Turner, M.B., Stewart, R.B., 2007. Improving the reliability of microprobe-based analyses of andesitic glasses for tephra correlation. The Holocene 17, 573–583.

Poidevin, J.-L., 1998. Les gisements d'obsidienne de Turquie et Transcaucasie: Géologie, géochemie, et chronométrie. In: Cauvin, M.-C., Gourgaud, A., Gratuze, B., Arnaud, N., Poupeau, G., Poidevin, J.-L., Chataigner, C. (Eds.). L'obsidienne au Proche et Moyen Orient: Du volcan à l'outil, Oxford, pp. 105–204.

Pollard, A.M., Blockley, S.P., Lane, C.S., 2006. Some numerical considerations in the geochemical analysis of distal microtephra. Applied Geochemistry 21, 1692–1714.

Pyle, D.M., Ricketts, G.D., Margari, V., van Andel, T.H., Sinitsyn, A.A., Praslov, N.D., Lisitsyn, S.N., 2006. Wide dispersal and deposition of distal tephra during the Pleistocene 'Campanian Ignimbrite/Y5' eruption, Italy. Quaternary Science Reviews 25, 2713–2728.

Sarna-Wojcicki, A.M., Pringle, M.S., Wijbrans, J., 2000. New $^{40}Ar/^{39}Ar$ age of the Bishop Tuff from multiple sites and sediment rate calibration for the Matuyama–Brunhes boundary. Journal of Geophysical Research 105, 21431–21443.

Sarna-Wojcicki, S., 2000. Tephrochronology. In: Sowers, J.M., Lettis, W.R., Noller, J.S. (Eds.), Quaternary Geochronology: Methods and Applications. American Geophysical Union, Washington, DC, pp. 357–377.

Shackley, M.S., 2008. Archaeological petrology and the archaeometry of lithic materials. Archaeometry 50, 194–215.

Shane, P., 2000. Tephrochronology: a New Zealand case study. Earth Science Reviews 49, 223–259.

Shane, P., Nairn, I.A., Martin, S.B., Smith, V.C., 2008. Compositional heterogeneity in tephra deposits resulting from the eruption of multiple magma bodies: implications for tephrochronology. Quaternary International 178, 44–53.

Shane, P., Smith, I., 2000. Geochemical fingerprinting of basaltic tephra deposits in the Auckland Volcanic Field. New Zealand Journal of Geology and Geophysics 43, 569–577.

Singer, B.S., Relle, M.K., Hoffman, K.A., Battle, A., Laj, C., Guillou, H., Carracedo, J.C., 2002. Ar/Ar ages from transitionally magnetized lavas on La Palma, Canary Islands, and the geomagnetic instability timescale. Journal of Geophysical Research 107, 2307.

Slimak, L., Kuhn, S.L., Roche, H., Mouralis, D., Buitenhuis, H., Balkan-Atli, N., Binder, D., Kuzucuoğlu, C., Guillou, H., 2008. Kaletepe Deresi 3 (Turkey): archaeological evidence for early human settlement in Central Anatolia. Journal of Human Evolution 54, 99–111.

Slimak, L., Roche, H., Mouralis, D., Buitenhuis, H., Balkan-Atli, N., Binder, D., Kuzucuoğlu, C., Grenet, M., 2004. Kaletepe Deresi 3 (turquie), aspects archéologiques, chronologiques et paléontologiques d'une sequence pléistocène en Anatolie centrale. Comptes Rendus Palevol 3, 411–420.

Stokes, S., Lowe, D.J., 1988. Discriminant function analysis of late Quaternary tephras from five volcanoes in New Zealand using glass shard major element chemistry. Quaternary Research 30, 270–283.

Stokes, S., Lowe, D.J., Froggatt, P.C., 1992. Discriminant function analysis and correlation of late Quaternary rhyolitic tephra deposits from Taupo and Okatina volcanoes, New Zealand, using glass shard major element composition. Quaternary International 13/14, 103–117.

Taşkıran, H., 2008. Réflexions sur l'Acheuléen d'Anatolie. L'Anthropologie 112, 140–152.

Taymaz, T., Yilmaz, Y., Dilek, Y., 2007. The geodynamics of the Aegean and Anatolia: introduction. In: Taymaz, T., Yilmaz, Y., Dilek, Y. (Eds.), The Geodynamics of the Aegean and Anatolia. Geological Society of London, London, pp. 1–16. Special Publication 291.

Toprak, V., 1998. Vent distribution and its relation to regional tectonics, Cappadocian Volcanics, Turkey. Journal of Volcanology and Geothermal Research 85, 55–67.

Tryon, C.A., Roach, N.T., Logan, M.A.V., 2008. The Middle Stone Age of the northern Kenyan Rift: age and context of new archaeological sites from the Kapedo Tuffs. Journal of Human Evolution 55, 652–664.

Turney, C.S.M., Blockley, S.P.E., Lowe, J.J., Wulf, S., Branch, N.P., Mastrolorenzo, G., Swindle, G., Nathan, R., Pollard, A.M., 2008. Geochemical characterization of

Quaternary tephras from the Campanian Province, Italy. Quaternary International 178, 288–305.

Turney, C.S.M., Lowe, J.J., 2001. Tephrochronology. In: Last, W.M., Smol, J.P. (Eds.), Basin Analysis, Coring, and Chronological Techniques. Tracking Environmental Change Using Lake Sediments, vol. 1. Kluwer Academic Publishers, Dordrecht, The Netherlands, pp. 451–471.

Verosub, K., Tchernov, E., 1991. Resultats preliminaries de l'étude magnetostratigraphique d'une sequence sedimentaire à l'industrie humaine en Israël. In: Vandermeersch, B. (Ed.), Les Premiers Peuplements de l'Europe. CNRS, Paris, pp. 237–242.

Yamei, H., Potts, R., Baoyin, Y., Zhengtang, G., Deino, A., Wei, W., Clark, J., Guangmao, X., Weiwen, H., 2000. Mid-Pleistocene Acheulean-like stone technology of the Bose Basin, South China. Science 287, 1622–1626.